The TESLA Post-linac Collimation System

R. Brinkmann, N. J. Walker

Deutsches Elektron–Synchrotron DESY, D-22603 Hamburg, Germany

G. A. Blair

Royal Holloway and Bedford New College, University of London, London, UK

TESLA-01-12

February 20, 2001

1   Introduction

In high-energy physics colliders, the 'halo' particles surrounding the core of the beams would cause intolerable background in the physics detectors if not removed. Collimation systems consisting of mechanical 'spoilers' on the order of a radiation length are placed close to the beam and used to 'scrape' the halo particles off: the particles scattered by the spoilers are then collected in ~ 20 radiation length 'absorbers', placed at suitable locations downstream of the spoilers. The absorbers are normally well within the optical shadow of the spoilers, so that the latter protects the former from a direct hit from the beam.

Collimation of the beam halo in the next generation of linear colliders is a complex and difficult problem. The first collimation system designs for a linear collider were proposed by the NLC group at SLAC [1], and have formed the basis of much of the work reported here. The high-energy of the halo particles (close to the beam energy, $250\,\mathrm{GeV}$) requires multiple-stage collimation; the extremely small beam emittances — and corresponding beam sizes — pose significant safety issues for the design of the mechanical spoilers: relatively large β-functions are generally required to increase the beam-sizes at the spoiler, to both enlarge the spoiler gap, and reducing the peak particle density on the spoiler if it is hit by the beam.

The TESLA concept [2, 3] has several advantages which relieve the constraints on collimation system:

- the large bunch spacing ($337\,\mathrm{ns}$) allows a head-on collision scheme using large aperture superconducting final doublets, which result in a relatively large required collimation depth ($13\sigma_x \times 80\sigma_y$, see section 2);

- the long bunch train (2820 bunches) and large bunch spacing allows the majority of the beam to be safely extracted in the event of some machine error or failure;

- the amount of halo expected from the superconducting linac is extremely small ($\sim 10^4$ particles per bunch, see section 3).

Since publication of the TESLA Conceptual Design Report (CDR) [2], the post-linac collimation system has undergone a major design change. The change reflects a shift in philosophy with respect to the machine protection issue: the system presented in the CDR [4] was based on the philosophy that all the spoilers should withstand a direct hit from a few design bunches of the bunch train. The system was characterised by large ($18\,\mathrm{km}$) β-functions, and the tolerances on magnet alignment and field quality were very tight. Unfortunately, this system was later shown not to be safe from damage from a large amplitude beam. The philosophy reflected in the new design is to protect the *momentum collimator* against a fast momentum error — e.g. klystron phase errors — since such events are the most probable (and frequent) failure modes for a linear accelerator. large amplitude betatron oscillations are by comparison rare events, and tend to be associated with magnet failures which are relatively slow (several milliseconds): a failure of a magnet could be detected by direct monitoring and the beam inhibited at the gun.
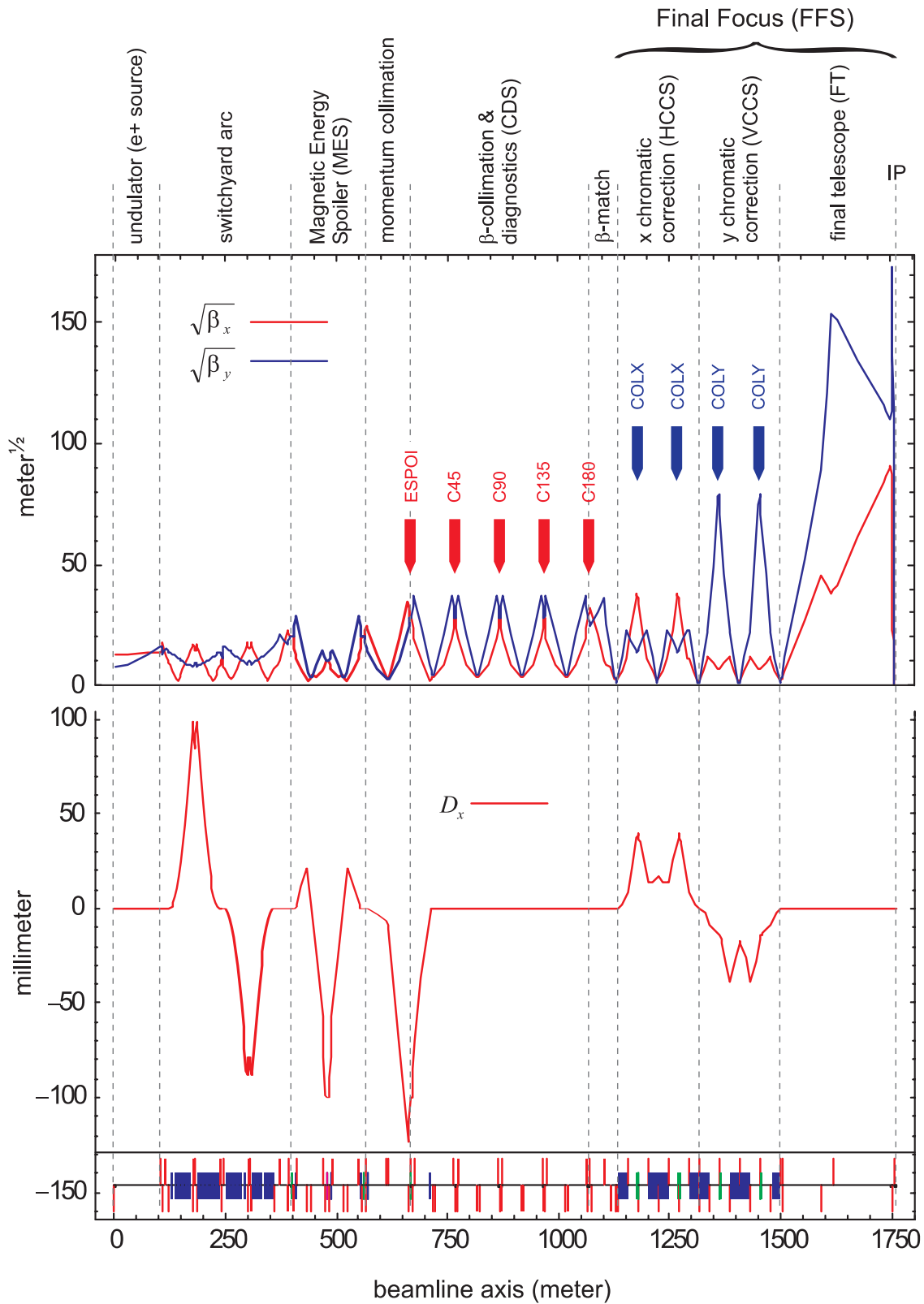
Figure 1: *Optics functions of the entire BDS. Locations of the spoilers (collimators) in the CDS and CCS sections are marked.*

The original beam delivery system had a separate diagnostics section (emittance measurement section, EMS) downstream of the collimation system. In the new system, the two systems have been combined into a single Collimation and Diagnostics System (CDS) to save space. Figure 1 shows the optics functions for the entire beam delivery system (BDS), including the CDS. The location of the various spoilers (collimators) are indicated. Upstream of the CDS is the magnetic energy spoiler (MES), which uses non-linear magnets to increase the beam size on the momentum (energy) spoiler (ESPOI) when the beam has a large ($< -1.5\%$) momentum error: it forms the basis of the fast-momentum error spoiler protection scheme (section 5.2). Not shown is the fast emergency extraction line (FEXL), which in the event of an error extracts the bunch train using fast kickers and transports it safely to the main dump. The FEXL is not covered here but is described in [5].

The following report reflects the current status of the design work on the collimation system. The work is on-going, and the design is subject to change. Section 2 briefly covers the required collimation depth set by the design of the interaction region (IR): it is this collimation depth that defines the upstream spoiler apertures. Section 3 estimates the halo population, based on several potential mechanisms. Sections 4 through 7 concentrate on the design and performance of the system itself:

- the basic lattice design is introduced in section 4;

- Section 5 covers spoiler protection issues, specifically GEANT studies of the interaction of the beam with the spoiler (section 5.1), and the concept of the magnetic energy spoiler (MES, section 5.2);

- section 6 presents an analysis of off-momentum trajectories in the complete BDS and an explanation of the second-order dispersion correction scheme, which was found to be necessary to prevent an off-momentum bunch from hitting a spoiler in the *betatron* collimation section;

- section 7 reports on the halo tracking studies using 'hard-edged' apertures (i.e. no particle scattering).

Although the tracking studies reported in section 7 are important, they do not give an indication of the efficiency of the collimation system. The spoilers do not 'stop' the particles, but instead scatter them in both angle and energy. A full simulation including scattering effects is required to make an estimate of the collimator efficiency; these studies will be done in the near future, and will be the subject of a second report. For completeness, however, section 8 briefly describes the scattering mechanisms and make some rough estimates of their effects. Finally, section 9 makes some brief comments concerning wakefields from the spoilers, and their potential degrading effect on the luminosity.
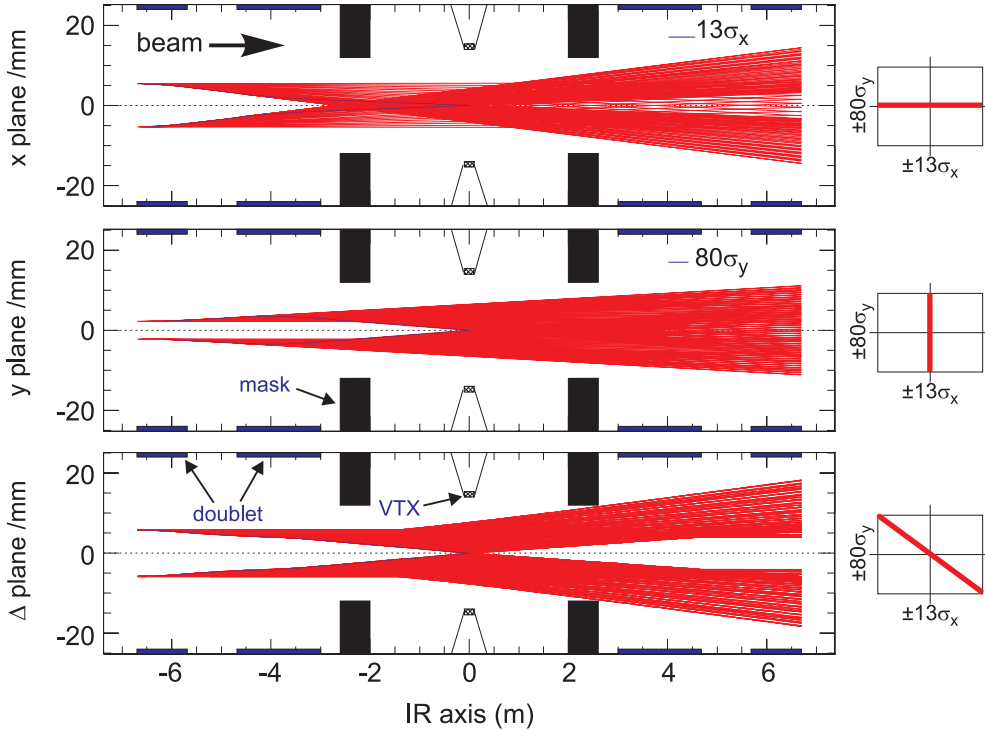
Figure 2: *Synchrotron radiation fan generated by the last quadrupoles and traced through the IR (taken from [6]). The envelope defines the required collimation depth of $\pm 13\sigma_x$ and $\pm 80\sigma_y$. The limiting aperture is defined in the diagonal (Δ) plane by the exit 24 mm mask.*

2 Required Collimation Depth

Halo particles with large amplitudes will radiate photons in the quadrupoles close to the IR; in particular, photons generated within the strong final doublet may strike inner parts of the detector and cause unacceptable background. The required collimation depth is defined as the aperture within which photons generated by halo particles pass cleanly through the IR.

The collimation depth for the current TESLA IR has been calculated in [6]. Figure 2 shows the limiting case for photons generated by an incoming halo in the final doublet; the resulting collimation depth is $\pm 13\sigma_x$ and $\pm 80\sigma_y$, where $\sigma_{x,y}$ are the nominal transverse beam dimensions at 250 GeV.

3 Estimate of Beam Halo

In this section we give a rough estimate of the amount of large-amplitude beam halo which has to be expected at the end of the main linac. The sources for halo which have been studied are large amplitude particles from the damping ring escaping the pre-linac collimation system, beam-gas scattering in the linac and dark current from field emission in the cavities. Intra-beam scattering was found to be an insignificant

source of halo generation in the linac. In the following we use as a definition for a halo particle one which has more than 30 standard deviations betatron amplitude in the vertical plane, corresponding to about half the acceptance of the BDS, or is outside the energy acceptance of about 1.5%.

3.1   Halo from damping ring

Although the damping ring is designed such that the core emittance of the beam is only slightly affected by beam-gas and intra-beam scattering, there is a non-zero population of the beam halo because of the extremely non-Gaussian nature of the particle distribution in the tails, caused by a small number of relatively hard scattering events. A pessimistic estimate for the fraction of halo particles from the damping ring is 10^{-3} of the total number of particles per bunch. The pre-linac collimation system will remove most of these particles. Since a detailed design of this system is not yet available, we have to estimate its efficiency from experience with the high-energy, post linac collimation system design. In previous studies [4] we found that less than 10^{-4} halo particles escape from a mechanical spoiler/absorber system at high beam energy. For the low-energy system the efficiency will likely be higher, but we use here the same value as a rough conservative estimate. Then, the number of halo particles injected into the main linac will be about $10^{-3} \cdot 10^{-4} \cdot N_e = 2 \cdot 10^3$ per bunch.

There is also the possibility that a certain fraction of charge will be stored in satellite RF-buckets before and after the main bucket. These particles would be accelerated in the linac with a large phase error and be outside the energy acceptance in the BDS (we are grateful to T. Raubenheimer for pointing out this potential problem). One way to avoid this large energy error would be to have the damping ring RF-system frequency at an integer fraction of the main linac frequency, so that the damping ring satellite buckets also match with the linac buckets.

3.2   Beam-gas scattering in the linac

The energy-dependent cross section for electrons (or positrons) Coulomb-scattering off gas nuclei (charge Z) with scattering angle larger n_σ standard deviations of the beam divergence can be written as:

$$\sigma(\gamma) \approx \frac{4\pi Z^2 r_e^2 \beta}{n_\sigma^2 \epsilon_y \gamma} \tag{1}$$

where $r_e = 2.8 \cdot 10^{-15}$m, $\beta \approx 100$m is the average beta function in the linac and $\epsilon_y = 3 \cdot 10^{-8}$m the normalised emittance. Assuming for the helium pressure at $2\,\mathrm{K}$ $p = 10^{-10}$mbar, the gas density (with Z=2) is about $3.6 \cdot 10^{14}/\mathrm{m}^3$. With $n_\sigma = 30$ the average number of scattering events per electron, integrated over the entire linac length, amounts to $5.7 \cdot 10^{-8}$. We thus obtain a halo population of about 10^3 particles per bunch. The effect of Bremsstrahlung due to beam-gas scattering has also been estimated and found negligible compared to the elastic scattering.

3.3   Dark current

Due to field emission in the cavities, a certain amount of dark current will be captured
by the RF-field and can be accelerated to high energies. Since the particles in the dark
current have much lower energies than the main beam, they will be over-focused by
the quadrupole lattice and most of them will rapidly reach betatron amplitudes large
enough to hit the cavity walls. In order to estimate the halo generated by dark current,
one has to determine the probability of survival of a field-emitted electron trajectory
over a large distance in the linac.

The process of initial capture and acceleration of field emitted electrons in a TESLA
cavity has been studied in [7]. We use these results to assess the approximate phase
space distribution of dark current at the exit of a 9-cell cavity at g=25 MV/m. It is
characterised by an absolute transverse emittance of about $4 \cdot 10^{-4}$m, an average energy
of 11 MeV and a phase spread of 40°. Using these parameters an initial distribution
of test particles was generated and tracked by computer simulation through the linac
components downstream. From the simulation, the probability of survival of a particle
trajectory, defined as staying within the cavity aperture, was derived. This probability
is a strong function of the position (i.e. nominal main beam energy) in the linac
where the electron was emitted (the further downstream in the linac, the stronger is
the over-focusing of the dark current). Using the 60° FODO lattice of the TESLA
linac, we determined the trajectory survival probability as a function of the nominal
beam energy E_0 at the cavity where the field emission takes place, see figure 3. The
data from the simulation can be approximated by a simple exponential function for
the survival probability (= number of stable trajectories divided by number of all
trajectories started):

$$\frac{n_{stable}}{n_{initial}} = \exp\left(-1.7(E_0/GeV)^{1.35}\right) \qquad (2)$$

Using this function one can perform an average over E_0 along the linac (taking into
account the first few GeV from the injection point upwards is sufficient due to the fast
decrease of the survival probability function). For an estimate of the absolute dark
current at the end of the linac, also the emitted dark current per cavity is needed. From
measurements of the cavity quality factor on the CW-RF test stand we can assume 1 μA
as a reasonable upper limit. As the final result, we then obtain the total dark current
at the end of the linac as a function of the linac injection energy, see figure 4. For
the design injection energy of 5 GeV the resulting dark current amounts to $3 \cdot 10^{-6}$ μA,
or $2 \cdot 10^4$ electrons per RF pulse, which corresponds to less than 10 halo electrons
per bunch. Even if this calculation can only be viewed as a rough approximation,
the transport of dark current to high energy does not seem to be a significant source
of beam halo in the BDS. It should be noted, though, that for lower linac injection
energies, the transported dark current can be several orders of magnitude higher. This
can be an issue for the FEL beam, which is accelerated from low energies to the final
energy without the insertion of a damping ring at the 5 GeV point. Further studies
are needed to asses the consequences for the FEL beam collimation system from these
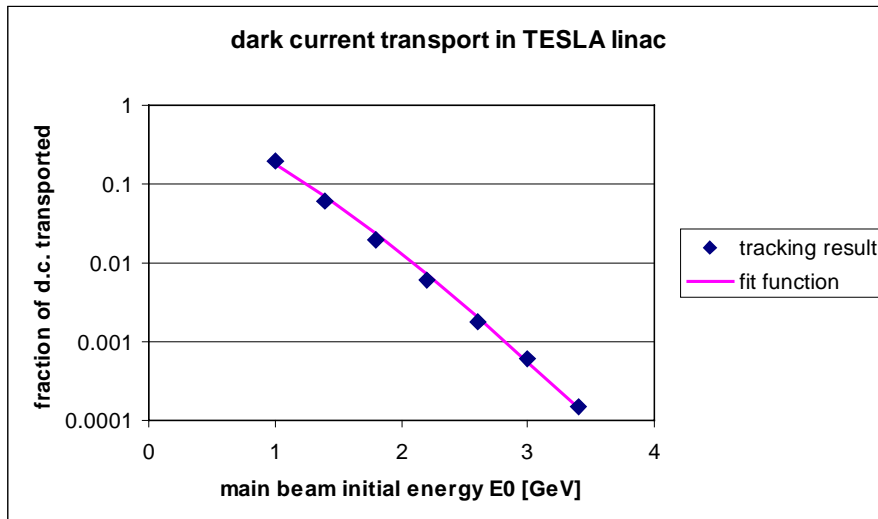considerations.

Figure 3: *Survival probability for trajectories of field-emitted electrons in the TESLA linac as a function of the cavity position (= nominal beam energy) in the linac.*

In summary, we conclude that from the sources considered here the expected number of halo particles is of the order of 10^3–10^4 per bunch.

3.4   Momentum spread of halo particles

From the above arguments, it is clear that the particles making up the halo cannot have an energy significantly different from that of the main beam. With a linac injection energy of 5 GeV we have seen that the two dominant particle sources are surviving halo from the damping ring and hard Coulomb scattered particles in the linac. For the latter, the particles can only be scattered to lower energies (i.e. $\delta < 0$), and we have seen that particles with more than a few % momentum deviation are extremely unlikely to be transported over any distance in the linac. The same argument applies for the surviving halo from the damping ring, with the exception that these particles can now have $\delta > 0$. For TESLA, the bunch is accelerated almost on crest, with only a small phase angle ($\sim 6°$) to compensate the effects of the longitudinal wakefield; thus halo particles can only have at the most $\sim 0.5\%$ higher energy than the main beam, which was taken as the upper limit in all the studies reported here.

4   Linear Lattice Design

The main (primary) collimation section (CDS) consists of a series of five identical cells, with $\beta_x = \beta_y = 800$ m at the symmetry points where the spoilers are located. The phase advance per cell (spoiler) is effectively $45°$ in both planes[1]. Figure 5 shows the

---

[1]due to optics constraints, the actual phase advance is $\phi_x = 45°$ and $\phi_y = 315°$.
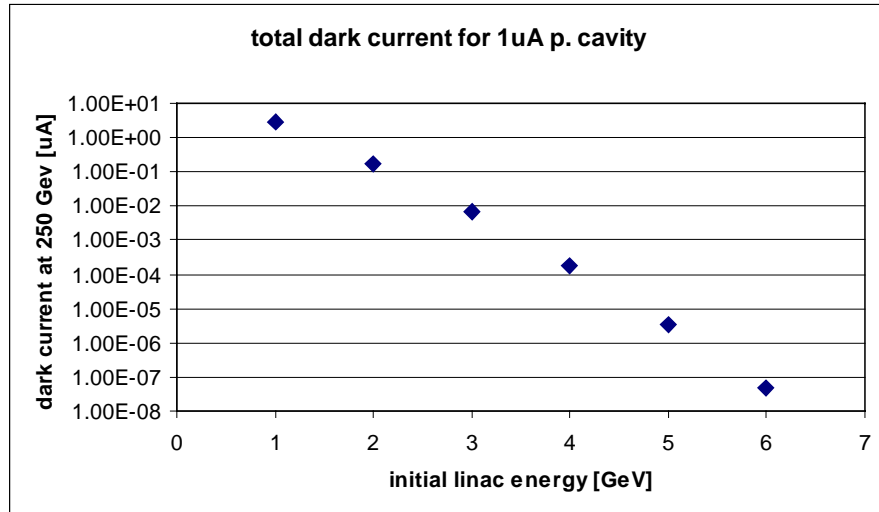
Figure 4: *Total dark current at the end of the main linac as a function of linac injection energy for an average field emission dark current of 1 µA per 9-cell cavity.*

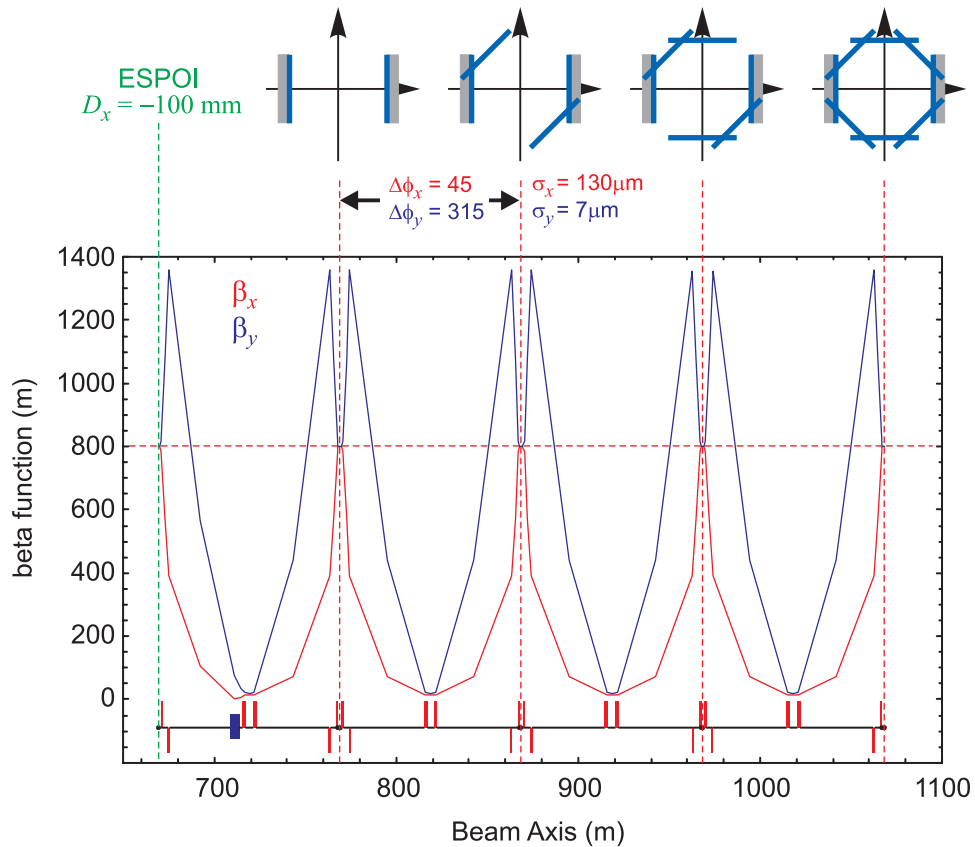Figure 5: *The primary collimation and diagnostics system (CDS).*

Spoiler	Aperture		Acceptance		
	x/mm	y/mm	$\pm x/\sigma_x$	$\pm y/\sigma_y$	$\pm\Delta P/P$ (%)
ESPOI	3	-	12	-	1.5
XYSPOI	3	1	12	74	-
COLX	3.9	0.6	13	80	5.7
COLY	0.9	2.7	13	80	2.9

Table 1: *Physical apertures (gaps) and the* linear *acceptance of the various spoilers in the BDS. ESPOI = energy spoiler, XYSPOI = betatron spoilers (CDS), COLX(Y) = CCS spoilers.*

optics. The first spoiler is at a high dispersion point ($D_x = -100$ mm), and is used as the momentum collimator. The remaining four spoilers are located in a zero dispersion region, and are referred to as the betatron collimation system; they effectively define an octagon in phase space as depicted in figure 5. The physical apertures of the spoilers are set to a factor $\cos(45°/2) \approx 0.92$ smaller than the required collimation depth, which fits the octagon defined by the spoilers inside the ellipse defined by the collimation depth. A second set of spoilers are located at the high β-points in the HCCS and VCCS; these collimators are positioned at the sine-like phase with respect to the IP, and so directly shadow the final doublet aperture. They are set to collimate exactly at $\pm 13\sigma_x$ and $\pm 80\sigma_y$. The physical apertures of all the spoilers are listed in table 1.

The last spoiler in the CDS is at the same phase as the first (momentum) spoiler; together they collimate a parallelogram in x-δ space (see figure 6), and *for a linear system* the total momentum collimation depth is $\pm 3\%$.

5   Spoiler Protection

The spoilers are by design the limiting apertures in the machine: when a bunch train comes out of the linac with a large orbit or energy error, it is the spoilers that should intercept the beam first. In the event of some upstream error, the fast emergency extraction line (FEXL) [5] should safely extract the beam after one or two bunches: hence the spoilers need only survive at most two bunches from the bunch train.

The original collimation system reported in [2, 4] reflected the philosophy that *all* spoilers should be able to survive a direct hit from some number of bunches. The beam size at each spoiler was blown up using linear optics to reduce the peak energy particle density to an acceptable level. The system was characterised by large (km) β-functions, resulting in relatively long systems with extremely tight tolerances. Such systems eventually proved to be impractical and have been abandoned. The current philosophy is to protect the spoilers from energy errors, since these are the most likely (frequent) type of error we can expect from the linac. Large orbit (pure betatron) oscillations of sufficient amplitude to strike a spoiler are probably rare events by comparison: the typical scenarios tend to be magnet failures, which occur relatively slowly (several milliseconds), and can be detected by direct monitoring.
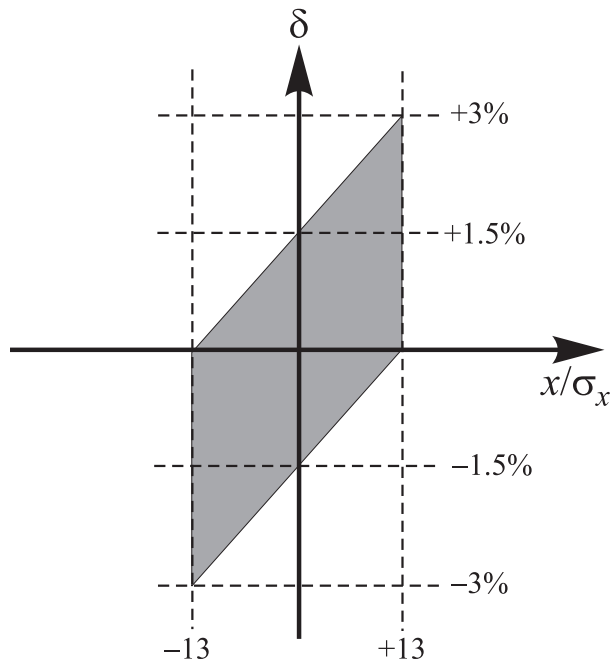
Figure 6: *The linear acceptance in the x-δ plane, defined by the first (momentum) and last horizontal spoilers in the CDS.*

5.1 Failure Limit for Spoilers

The interaction of a bunch with a spoiler was investigated using `GEANT3`, where a 250 GeV beam of electrons was fired into two radiation lengths of titanium , i.e. 2×3.56 cm. The bunch was taken as a Gaussian distribution in x and y, with rms parameters $\sigma_x = 130\sqrt{\mathcal{M}}$ μm and $\sigma_y = 7\sqrt{\mathcal{M}}$ μm where $\mathcal{M}$ is a magnification factor, $\mathcal{M}$=1 for the nominal bunch size at the spoiler.

A sensitive volume was defined to be a box with x y-dimensions respectively of σ_x, σ_y and divided into 20 longitudinal segments in z, each of length $X_0/10$. In this way the energy deposition close to the z-axis of the bunch is determined. The Gaussian distribution leads to 0.147 of the bunch entering the sensitive volume. The setup is illustrated in figure 7.

The specific heat capacities of titanium and graphite were obtained from the formula given in [8]:

$$C_p = a + bT + dT^{-2} \qquad (3)$$

and the parameters are listed in table 2. If we take the criterion arising from ultimate tensile strength (UTS) considerations, quoted in [4], that the instantaneous change in temperature should not exceed 1000 K for titanium and 2650 K for graphite, this translates into an upper limit on the allowed instantaneous energy deposition of 635 J/g and 5.10 kJ/g respectively.

A sample of 10^6 particles were simulated for each of the cases $\mathcal{M}$=1, 2, 10 and
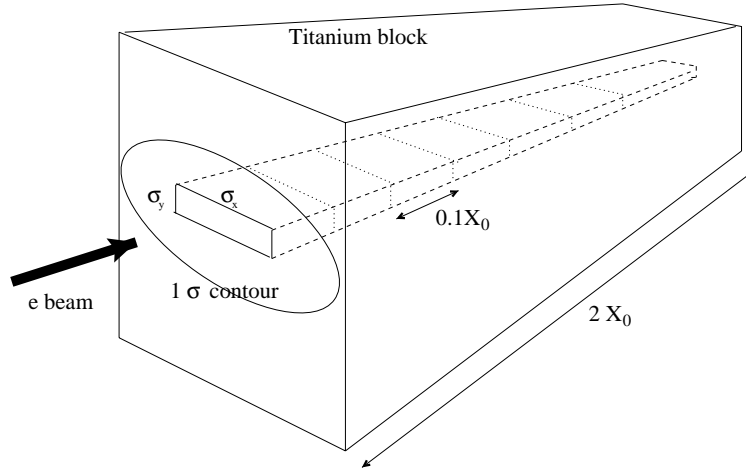
Figure 7: *Setup of the* `GEANT3` *model. The x and y dimensions of the titanium block are much larger than shown, so as to allow the electromagnetic shower to develop fully. The sensitive volume is centred on the beam transverse profile so as to record the maximum energy density deposited by the bunch. The dimensions of the sensitive volume correspond to 1 σ_{bunch} in both x and y.*

Material	$a(J/gK)$	$b(J/gK^2)$	$d(\mathrm{JK/g})$	$\Delta T_{\mathrm{UTS}}(K)$	$(dE/dm)_{\mathrm{max}}(J/g)$
Titanium	0.459	$2.20\ 10^{-4}$	0	1000	635
Carbon	1.43	$3.56\ 10^{-4}$	$-7.32\ 10^{4}$	2650	5100

Table 2: *Spoiler material characteristics.* ΔT_{UTS} *is the maximum temperature allowed arising from UTS considerations and* $(dE/dm)_{\mathrm{max}}$ *is the corresponding maximum allowed energy deposition.*

the energy deposition scaled to the nominal bunch occupancy of 2×10^{10} particles and the results are shown in figure 8. To check the normalisation, the energy loss from a single $250\,\mathrm{GeV}$ muon is shown in figure 9, where the effect of multiple scattering is illustrated at larger penetration depths for both carbon and titanium. The energy loss at small penetration depths agrees with the plots in figure 8, as expected because at these depths the energy loss by electrons is due to ionisation alone. (Note, in making this comparison, it is important to remember that only 14.7% of the electrons in the Gaussian bunch lie within a $1\sigma \times 1\sigma$ box in the transverse plane that defines the sensitive volume.)

Figure 8(a) shows the limit from UTS for titanium; as a comparison, figure 8(b) shows the results for carbon (graphite). It is clear from the figure that a $2X_0$ Ti spoiler is at the UTS limit for only one bunch, assuming the nominal beam size ($\mathcal{M}$=1). Extracting the maximum energy deposition for titanium and graphite from figure 8 as 585 J/g and 202 J/g respectively, we conclude that the numbers of bunches which could be sustained at the same spot are 1 and 25 respectively. For one radiation length of Ti the energy deposition per gram is less than for two, but the results still suggest
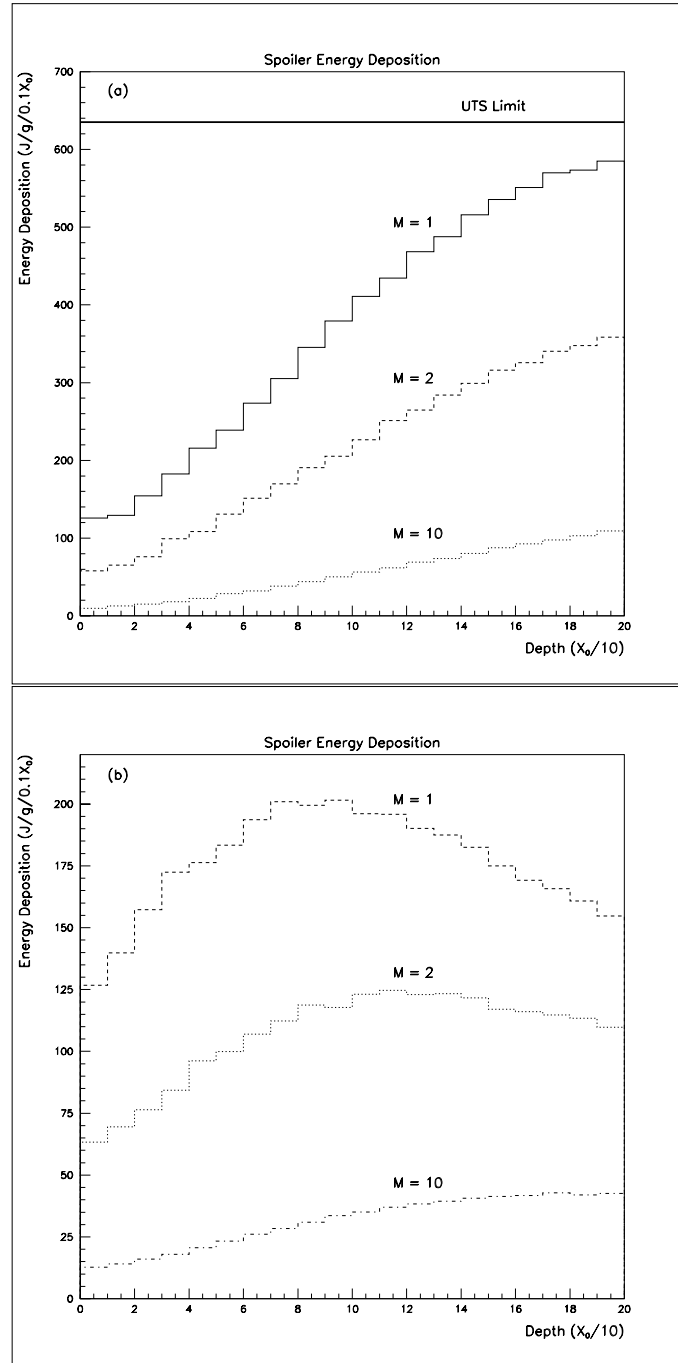
Figure 8:   *Energy deposition in the spoiler from a single bunch, as a function of longitudinal position for beam-spot magnification factors $\mathcal{M}$=1,2,10. (a) is for titanium and (b) is for carbon. Each z-bin corresponds to 0.1 radiation length. For titanium, the upper limit imposed by UTS requirements is also shown.*
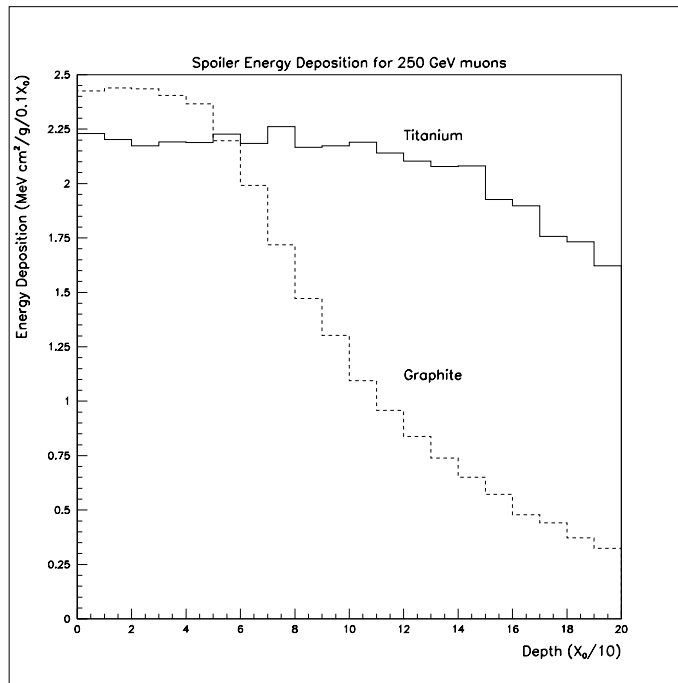
Figure 9:   *Energy deposition in the spoiler from a single muon, as a function of longitudinal position for titanium and carbon. The plots illustrate the effect of multiple scattering, causing the muon to exit the sensitive volume.*

that two bunches would be sufficient to exceed the UTS limit.

For comparison with previous studies [4] the simulation was repeated using the old TESLA parameters and the results shown in figure 10.

5.2   Magnetic Energy Spoiler (MES)

The fast emergency extraction scheme should in principle only allow one bunch of the bunch train to pass through, extracting the remaining train to the main dump. The GEANT studies described in the previous section suggest that one radiation length titanium spoilers could withstand one or two direct hits from a bunch *with the design beam parameters*, i.e. $\sigma_x = 130\,\mu\text{m}$, $\sigma_y = 7\,\mu\text{m}$, $N_{\text{bunch}}=2 \times 10^{10}$. However, recent experiments using the SLAC linac have indicated that failure tends to occur at lower instantaneous power densities than the GEANT studies would suggest [9], and so an additional level of protection seems prudent.

A non-linear magnet system referred to as the magnetic energy spoiler (MES) is incorporated just upstream of the collimation system. Figure 11 indicates how the system works. An off-momentum bunch receives a horizontal kick from the octupole at the high dispersion point ($D_x = -100\,\text{mm}$), which translates into a (momentum dependent) horizontal offset at the downstream skew-sextupole[2]. The effective *skew-*

---

[2]the octupole effectively generates third-order dispersion at the skew-sextupole.
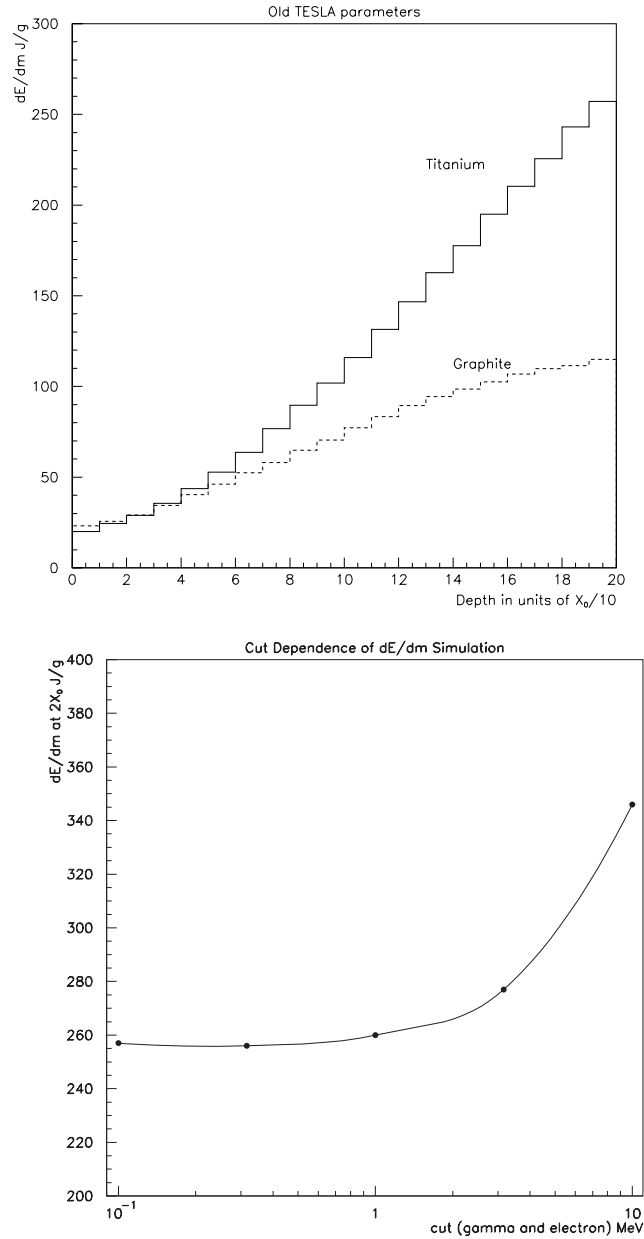
Figure 10:   *The top plot shows the energy deposition in the spoiler from a single bunch, as a function of longitudinal position for the original CDR TESLA parameters ($\sigma_x = 158\,\mu m$, $\sigma_y = 59\,\mu m$, $N_{\rm bunch} = 3.6 \times 10^{10}$). The differences from previous calculations could be attributed to the cut parameters used in the simulation. The dependence on the GEANT cut parameters (for photons and electrons) is shown in the bottom plot (generated with lower statistics of 10^4 events per point). Throughout this paper the default cut value of 1 MeV is used, which is clearly consistent with lying on the plateau of this figure.*
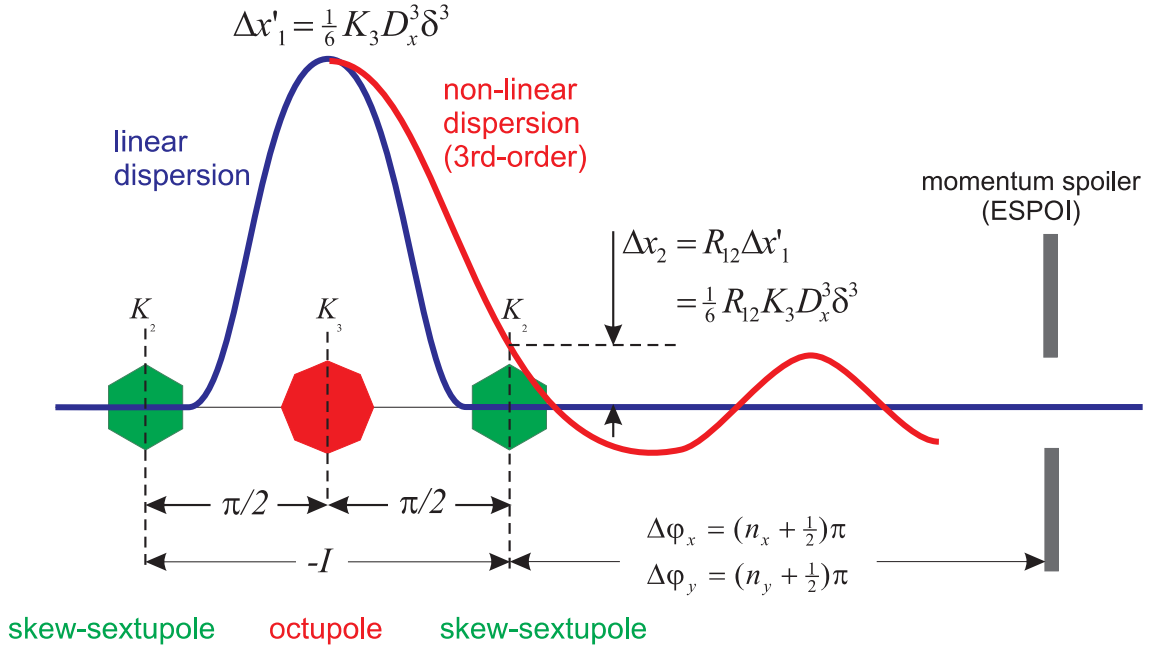
$$\Delta x'_1 = \tfrac{1}{6} K_3 D_x^3 \delta^3$$

non-linear
dispersion
(3rd-order)

linear
dispersion

momentum spoiler
(ESPOI)

K_2 K_3 K_2

$$\Delta x_2 = R_{12}\Delta x'_1$$
$$= \tfrac{1}{6} R_{12} K_3 D_x^3 \delta^3$$

$$\longleftarrow \pi/2 \longrightarrow \hspace{-2pt} \longleftarrow \pi/2 \longrightarrow$$

$$\longleftarrow \hspace{3cm} -I \hspace{3cm} \longrightarrow$$

$$\Delta\varphi_x = (n_x + \tfrac{1}{2})\pi$$
$$\Delta\varphi_y = (n_y + \tfrac{1}{2})\pi$$

skew-sextupole   octupole   skew-sextupole

Figure 11: *Concept of the magnetic energy spoiler (MES). See text for details.*

quadrupole generated couples the horizontal emittance into the vertical plane. The result is a significant increase in the vertical beam size at the momentum spoiler, placed $(n + 1/2)\pi$ downstream in both x- and y-phase. From a simple thin-lens analysis (see Appendix A), the increase in vertical beam size at the spoiler as a function of momentum error $\delta = \Delta p/p$ is

$$\frac{\sigma_y(\delta)}{\sigma_y(\delta = 0)} \approx \frac{1}{6} K_2 K_3 R_{12} \sqrt{\beta_x \beta_y} \sqrt{\frac{\epsilon_x}{\epsilon_y}} D_x^3 \delta^3 \tag{4}$$

where K_2, K_3 are the integrated strengths of the skew-sextupoles and octupole respectively, D_x is the linear dispersion at the octupole, R_{12} is the linear Green function from the octupole to the skew-sextupole, and $\beta_{x,y}$ are the β-functions at the skew-sextupole. The system also generates centroid kicks to the beam, resulting in third-order horizontal dispersion and sixth-order vertical dispersion. These energy dependent orbits eventually cause the beam to hit a betatron collimator in the CDS section. If the collimator apertures are set at $\pm N_x\sigma_x$ and $\pm N_y\sigma_y$, the maximum relative increase in beam size, defined at the point when the beam hits a betatron spoiler, is given by

$$\left.\frac{\sigma_y(\delta)}{\sigma_y(0)}\right|_{max} \approx 2\frac{N_y}{N_x} \tag{5}$$

For the current system, the limit corresponds to $2 \times (80/13) \approx 12$. However, chromatic effects in the downstream CDS lattice not included in the above analysis constrain the maximum obtainable factor still further. The current values of $K_2 = 5\,\mathrm{m}^{-2}$ and $K_3 = 640\,\mathrm{m}^{-3}$ are set to give a factor of $\sim$6 increase in vertical beam size, which has
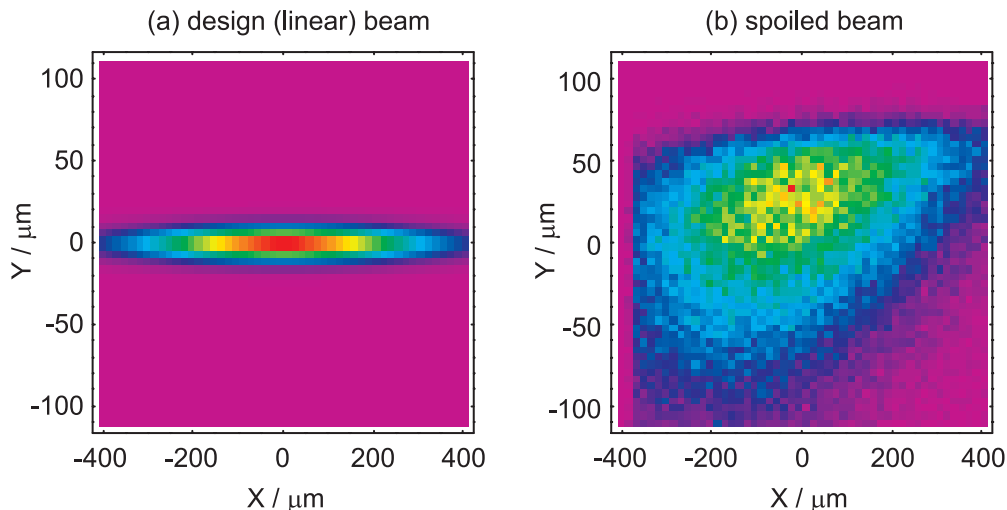
Figure 12: *Results of tracking a design beam with a momentum centroid error of $\Delta P/P = -2\%$. (a) shows the* design *beam on the energy spoiler (ESPOI), while (b) shows the results of the tracking. The beam area is increased by a factor of 6.*

been confirmed using tracking (see figure 12).

6   Analysis of Off-Momentum Trajectories

The relatively strong chromaticity, coupled with the non-linear elements in the magnetic energy spoiler (MES), tend to generate very high orders of dispersion in the collimation sections and beyond. The simple thin-lens analysis of the MES reported in section 5.2 and described in detail in appendix A is not sufficient to safely predict the behavior of an off-momentum beam. In particular, the simple model assumes only linear transfer between the non-linear elements and the spoilers; in reality the chromaticity of the quadrupoles plays a significant role. One particularly important contribution comes from the quadrupoles adjacent to the octupole at the high dispersion point in the MES: if left uncorrected, these quadrupoles generate a significant second-order dispersion which interferes with the (design) third-order dispersion from the octupole. We shall see that to control the non-linear dispersion in the CDS section requires compensation of the second-order dispersion generated at each high dispersion point in the upstream system.

To analyse the chromatic behavior of the system to high order, we have used *Mathematica* [10] to track truncated power series in $\delta = \Delta p/p$ through the beamline. A six-vector was tracked with the following initial value:

$$\vec{X}_0 = (0, 0, 0, 0, 0, \delta + O(\delta^n)) \tag{6}$$

where $\delta + O(\delta^n)$ indicates that the momentum coordinate is a power series to order n. Typically n was taken as 12. The multipole strengths of the magnets were also

expanded to n^{th}-order in δ using the following series:

$$\frac{1}{1+\delta} \approx 1 - \delta + \delta^2 - \delta^3 + \ldots + O\left(\delta^n\right) \tag{7}$$

Each quadrupole was represented by a 6×6 matrix $\mathbf{R}$:

$$\mathbf{R} = \mathbf{R_0} + \mathbf{R_1}\delta + \mathbf{R_2}\delta^2 + \mathbf{R_3}\delta^3 + \ldots \tag{8}$$

Sextupoles and octupoles were treated as thin-lens kicks, again with their multipole strengths expanded in δ to n^{th}-order.

The tracked vector was stored after each element in the beamline; at each location the vector represents the non-linear dispersion to n^{th}-order.

Figure 13 shows the results of the calculation for the design beamline with no second-order correction. The plot shows the off-momentum trajectories for $-1.5\% \leq \delta \leq +0.5\%$. The lower limit of -1.5% represents the linear collimation momentum aperture of the momentum spoiler. The plots clearly show a resonant-like growth of the amplitude due to the non-linear chromatic effects. The vertical behavior is a result of the skew-sextupole in the MES, which by design generates sixth-order vertical dispersion (see Appendix A). The strong non-linear behavior causes the momentum acceptance of the system to be defined by the betatron collimation spoilers in the CDS, downstream of the design momentum collimator at the high (linear) dispersion point. Figure 14 shows the horizontal and vertical dispersion at the five spoiler locations. The horizontal dispersion at the momentum spoiler (ESPOI) is still dominated by the design linear dispersion ($D_x = -100\,\text{mm}$), and defines the (design) lower momentum aperture at -1.5%. The plots for C135 and C180 show that a beam with a momentum error of $\sim -1.2\%$ would hit these spoilers first, which is clearly undesirable: the smaller momentum acceptance significantly reduces the effectiveness of the MES[3], since the relative increase in beam size is proportional to δ^3. In addition, the C135 spoiler is at the wrong phase and would see a significantly smaller vertical beam size.

To understand the driving mechanism for the non-linear behavior, and to identify the terms which dominate, each order of dispersion was analysed separately to evaluate its contribution to the total effect. To clearly identify the 'sources' of the non-linear terms, a *normalised* dispersion ($\zeta_{x,n}$) was calculated for each term as follows:

$$\zeta_{x,n} = \frac{\delta^n_{\text{ref}}}{\sqrt{\epsilon_x}}\sqrt{\gamma_x d^2_{x,n} + 2\alpha_x d_{x,n}dx', n + \beta_x d^2_{x',n}} \tag{9}$$

where the $d_{u,n}$ are the coefficient of the δ^n term in the power series for the coordinate $u \in \{x, x', y, y'\}$, e.g.

$$
\begin{aligned}
x(\delta) &= d_{x,0} + d_{x,1}\delta + d_{x,2}\delta^2 + \ldots \\
x'(\delta) &= d_{x',0} + d_{x',1}\delta + d_{x',2}\delta^2 + \ldots
\end{aligned}
$$

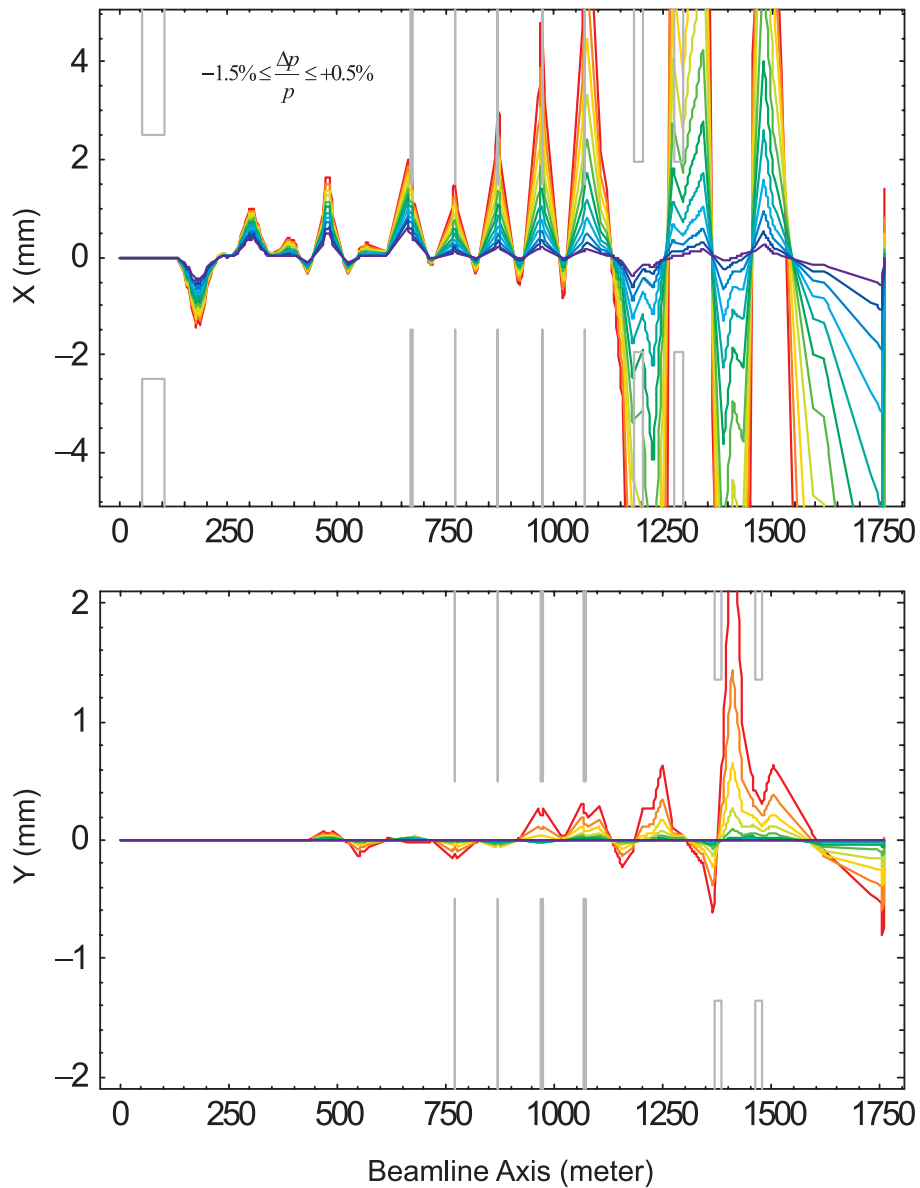[3]the beam could hit the spoiler with a smaller momentum error

Figure 13: *Off-momentum trajectories through the entire BDS with no second-order compensation. Each trajectory is colour coded with red representing $\delta = -1.5\%$ and blue representing $\delta = +0.5\%$. The gray lines represent the physical apertures of the beamline, including the spoilers (visible). The trajectories are based on a semi-analytical calculation of the 12th-order δ-dependent map.*
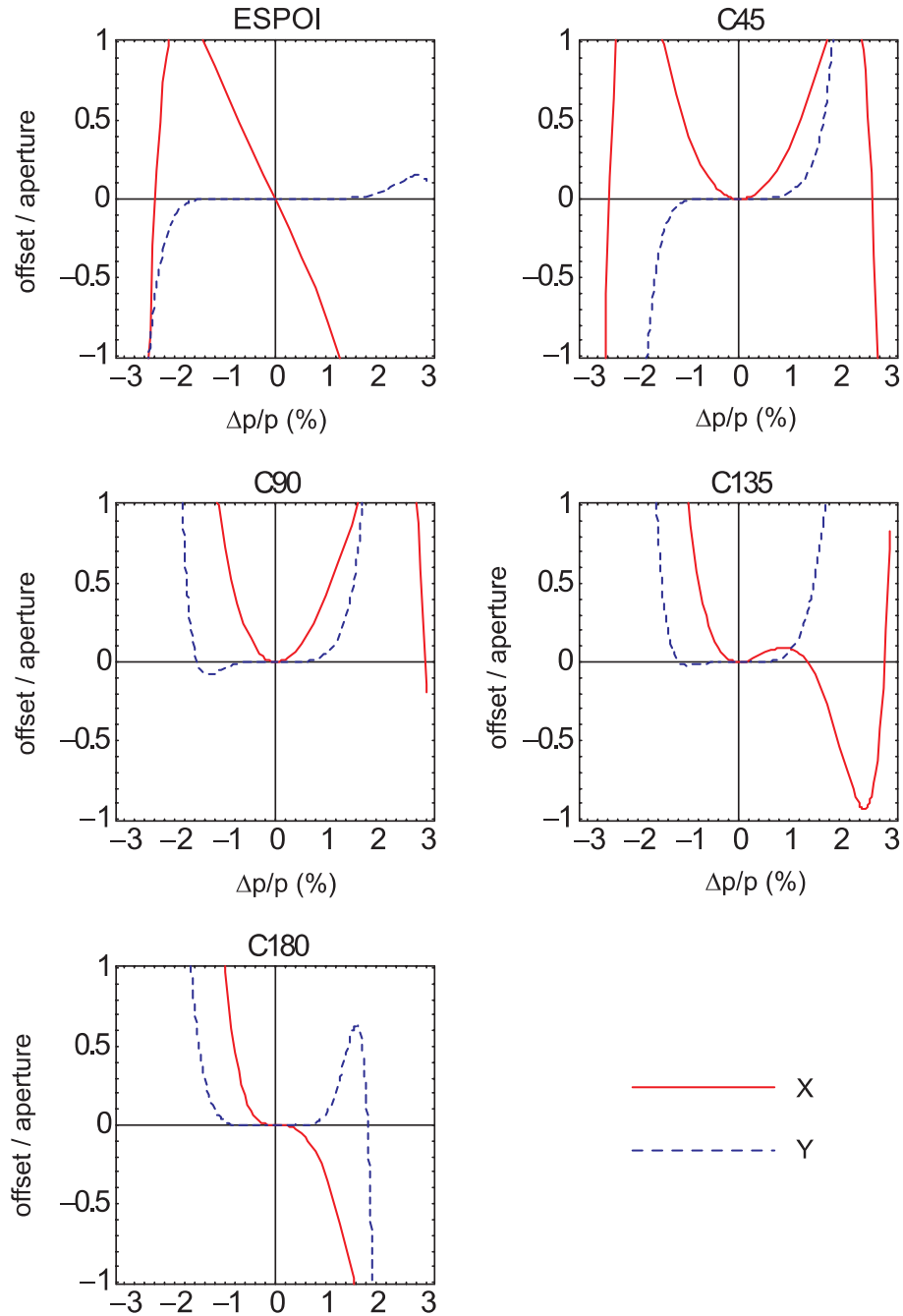
Figure 14: *Dispersive behavior at the momentum collimator (ESPOI) and the four down-stream betatron collimators, labels CN, where N indicates the design phase advance from ESPOI. No second-order compensation is included. The vertical scale (offset) is normalised to the spoiler aperture in the respective plane: hence a value of ± 1 represents the spoiler edge. The plots are based on a semi-analytical calculation of the 12th-order δ-dependent map.*
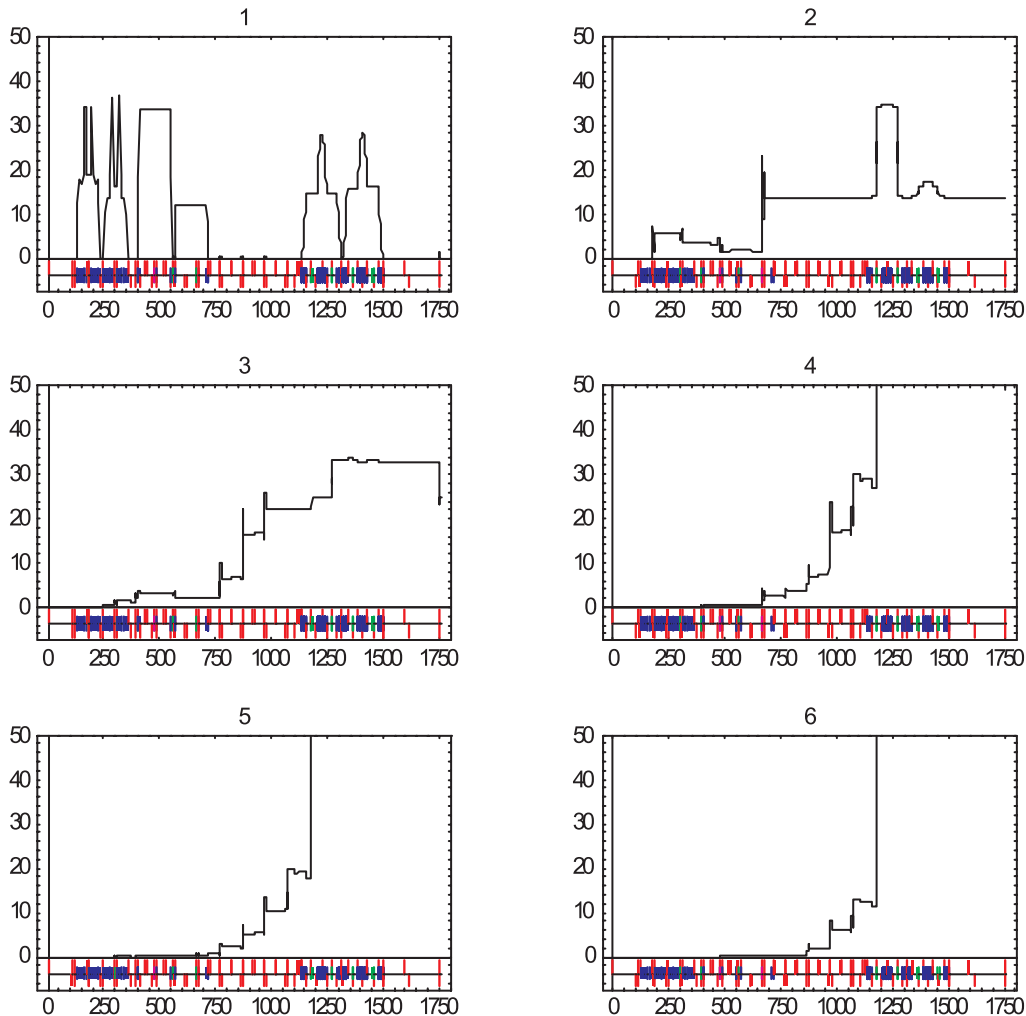
Figure 15: *Plots of the normalised horizontal n^{th}-order dispersion ($\zeta_{x,n}$) for $n = 1 \ldots 6$.*

δ_{ref} is the reference momentum, and was generally taken as -1.5%. Normalising by the square root of the emittance ($\sqrt{\epsilon_x}$) gives the results in terms of the nominal (linear) beam size. The important feature of this normalised dispersion is that it remains at a constant value if there are no generating sources for that term.

Figure 15 shows the results for $n = 1 \ldots 6$ for the horizontal (x) plane; figure 16 shows the corresponding values of $\zeta_{y,n}$ for $n = 4 \ldots 9$. In figure 15, the $n = 1$ plot represents the design linear dispersion[4]. The $n = 3$ plot should show a single step at the octupole in the MES ($z \approx 500 \, \text{m}$) and then remain constant: the observed gradual growth is due to the spurious second-order dispersion ($n = 2$ plot), which in combination with the chromaticity of the quadrupoles drives the third-order dispersion.

---

[4]we can see from this plot that a $\delta = -1.5\%$ causes an offset in the (linear) dispersive regions of 10–$40\sigma_x$
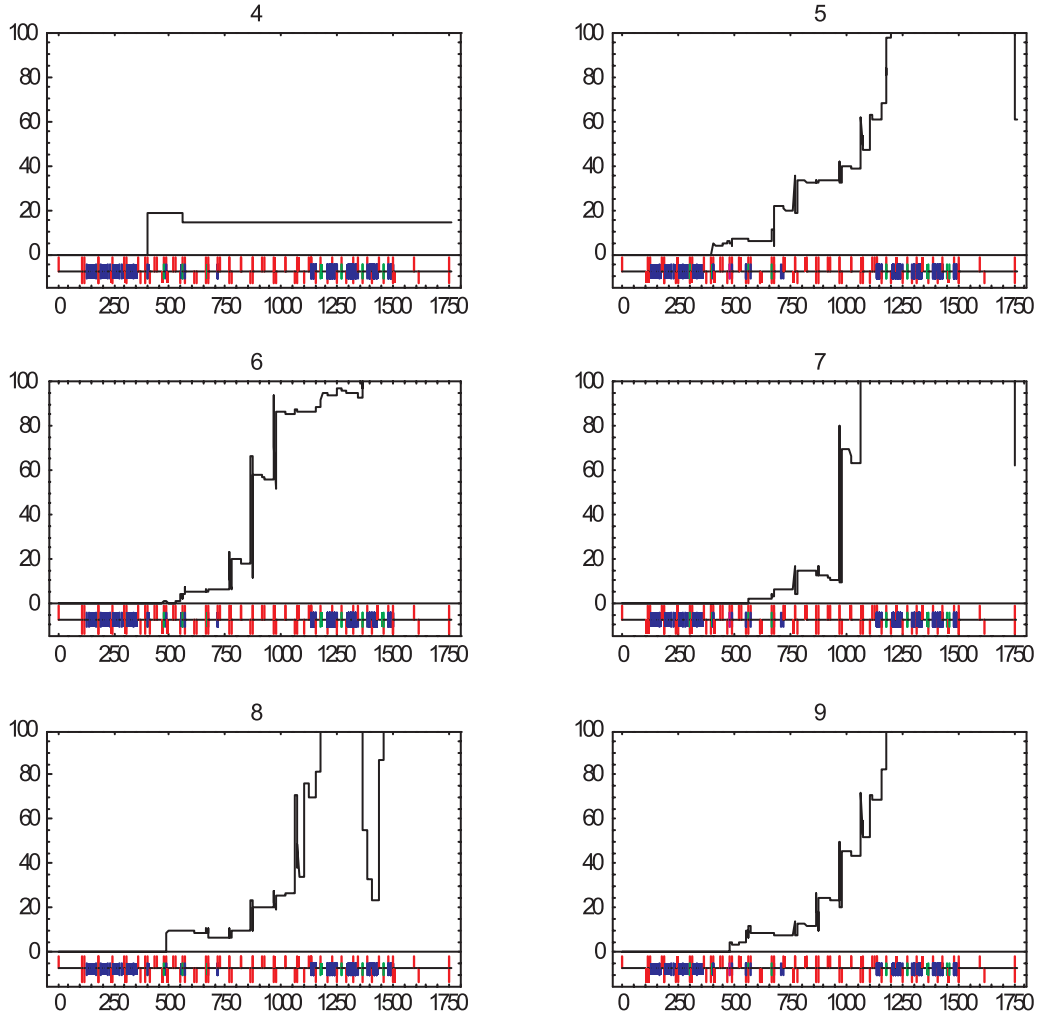
Figure 16: *Plots of the normalised vertical n^{th}-order dispersion ($\zeta_{y,n}$) for $n = 4 \ldots 9$.*

Generally speaking, each order n drives the $n + 1$ order via chromaticity. The corresponding plots for the vertical plane (figure 16) should show a step function in the $n = 6$ plot at the location of the second skew-sextupole ($z \approx 520$ m). The presence of fourth-order vertical dispersion ($n = 4$ plot) is again due to the non-zero second-order horizontal dispersion at the skew-sextupoles.

To correct the second-order horizontal dispersion (and therefore suppress the higher-order terms), four weak sextupoles where located at the following high dispersion points:

- two sextupoles at the two high dispersion peaks in the switch-yard arcs, which zero the second-order dispersion at the first skew-sextupole;

- one sextupole next to the octupole in the MES, which cancels the second-order

term at the second skew-sextupole;

- a final sextupole at the location of the momentum spoiler, which cancels the effects in the downstream CDS.

Figures 17 through 20 show the plots corresponding to the previous figures (13–16) with the four sextupole compensations scheme. As expected, the correction of the second-order term has significantly reduced the generation of high-order terms. In particular, the collimation aperture is now correctly defined at -1.5% by the momentum collimator (see figures 17 and 18).

It is important to note that the effects of additional betatron-like oscillations are not included in the above analysis. This reflects the design philosophy that the system should be made safe against momentum errors which are considered the most likely failure mode of the machine. It is clear, however, that a betatron component will play a role, and that is likely that the beam will have some betatron component in the event of a failure. In addition, we must take into account the large betatron amplitudes when considering the halo, which the collimation system is designed to remove.

The semi-analytical approach for the δ-dependent map could in principle be expanded to a multivariate analysis including all the phase space coordinates (x, x', y, y'). Unfortunately dealing with the extremely large number of terms generated becomes time and memory intensive, and traditional particle tracking becomes the only realistic option.
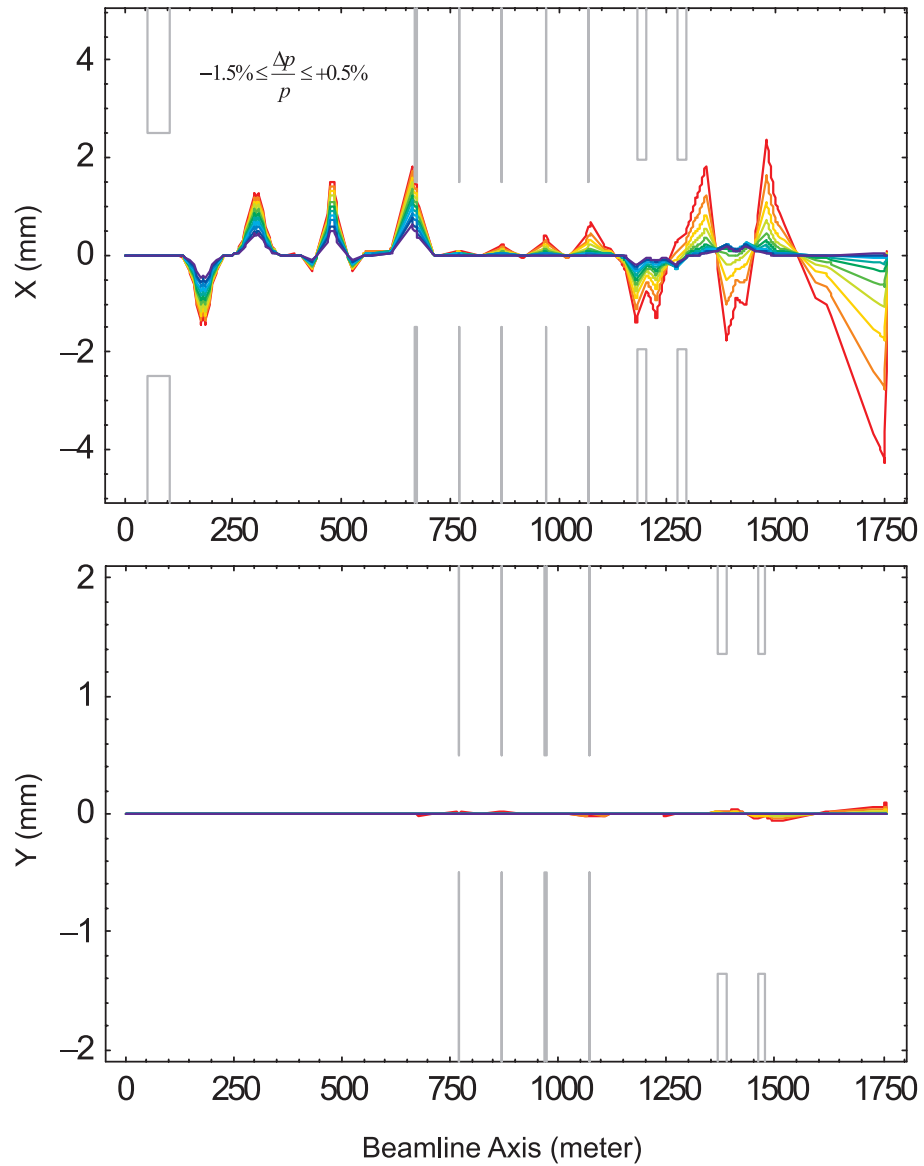
Figure 17: *Off-momentum trajectories through the entire BDS with second-order compensation (see fig. 13 for more details).*
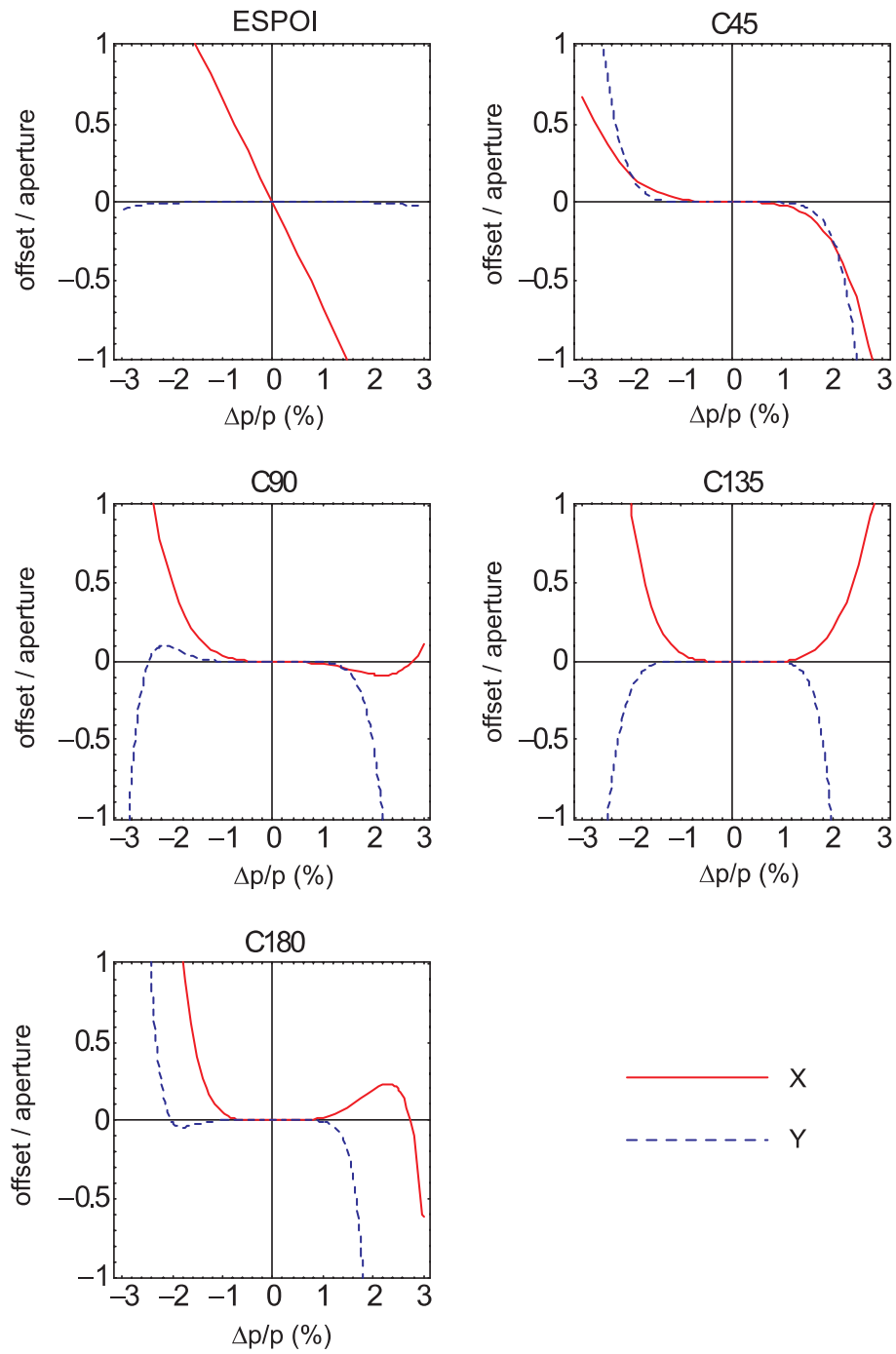
Figure 18: *Dispersive behavior at collimators with second-order compensation included (see fig. 14 for more details).*
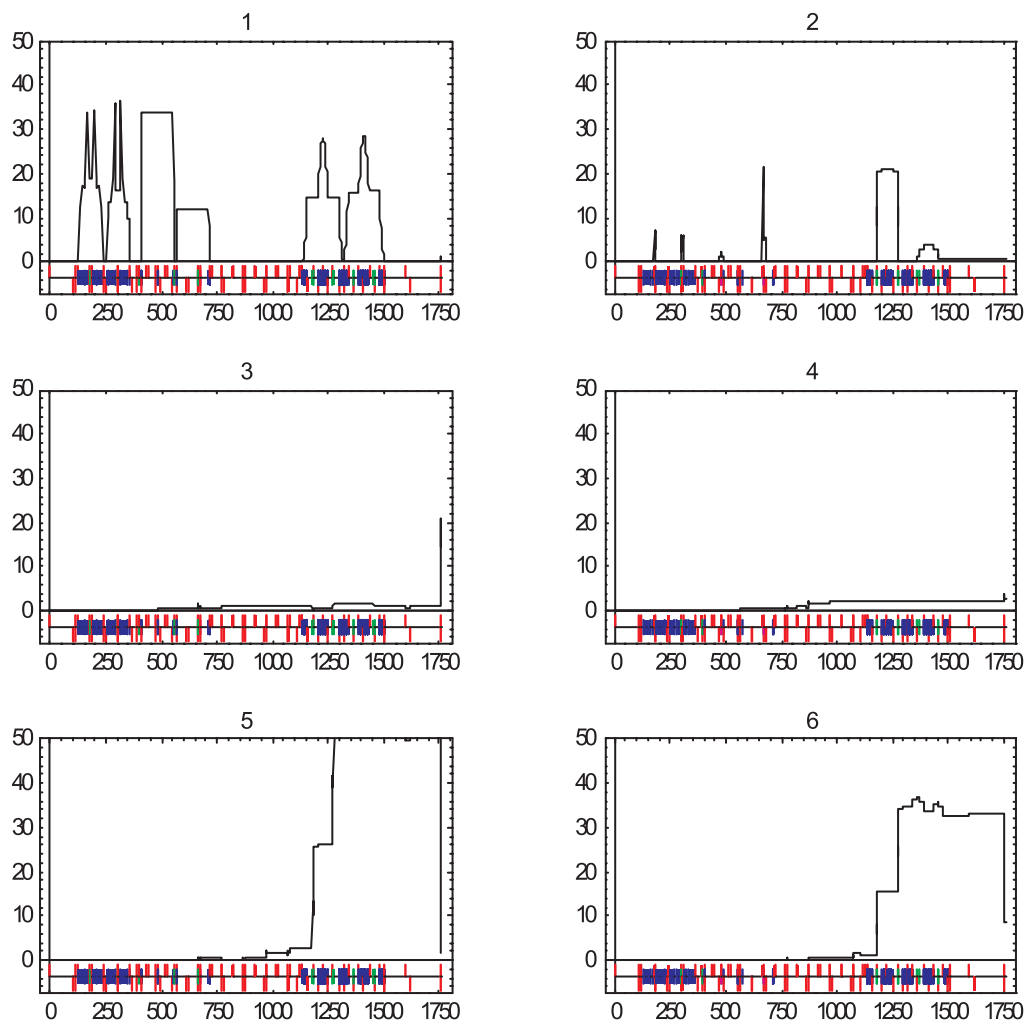
Figure 19: *Plots of the normalised horizontal n*th*-order dispersion ($\zeta_{x,n}$) for n = 1 . . . 6 with second-order compensation.*
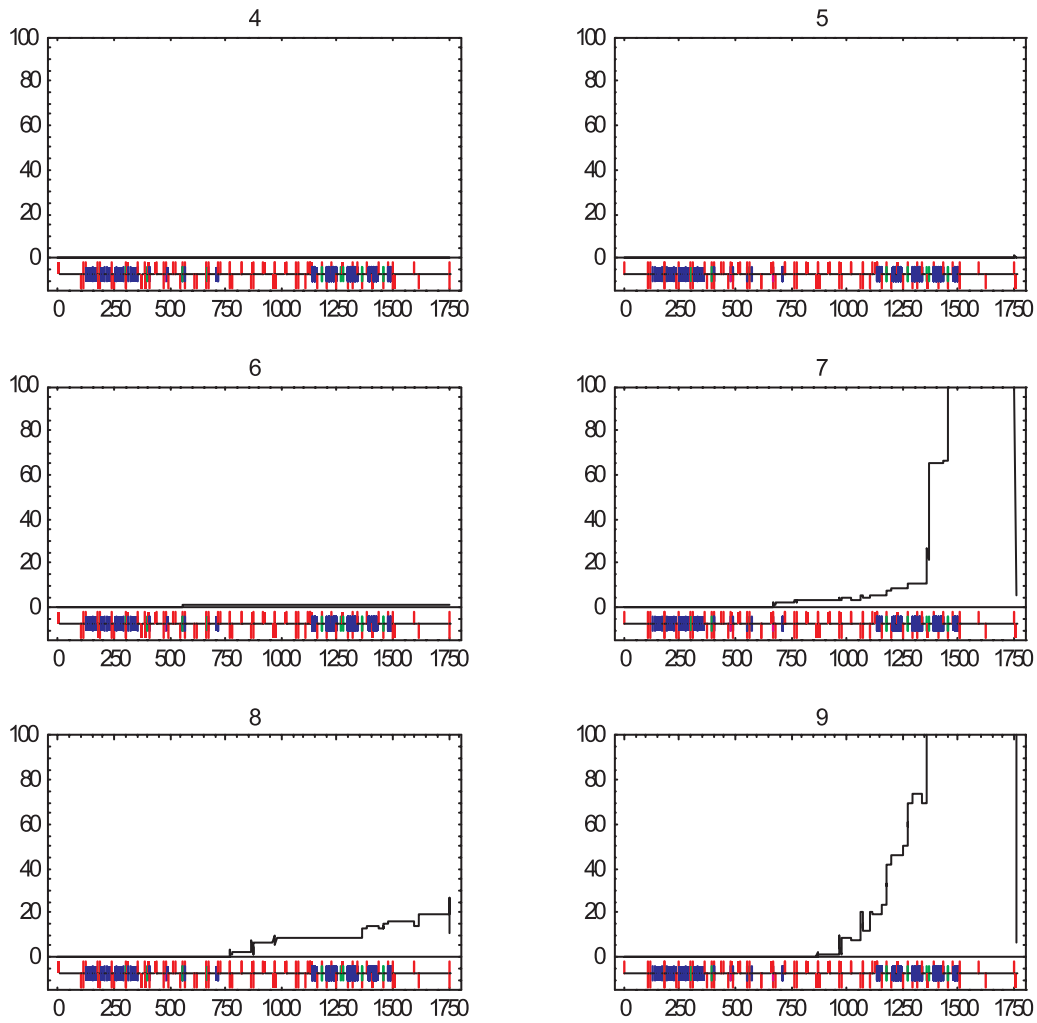
Figure 20: *Plots of the normalised vertical n^{th}-order dispersion ($\zeta_{y,n}$) for $n = 4\ldots 9$ with second-order compensation.*

7   Tracking Simulations

Tracking simulations of the halo were performed using a model constructed with the `MERLIN-II` C++ class library [11]. The studies reported here are concerned only with the *dynamic aperture* of the system, and not directly with the collimator efficiency. Dynamic aperture studies involve simple particle tracking of a halo with hard edged apertures, where a particle is deemed 'lost' if outside a given aperture; such studies are the first step to evaluating the effectiveness of the collimation system, since they:

- indicate where *primary* particles will first encounter an aperture;

- show that the required collimation aperture (depth) at the doublet (section 2) is inside the 'dynamic' shadow of the upstream spoiler apertures.

By design, the spoiler apertures are set to shadow the doublet to the correct depth for a *linear* system: however, the strong non-linearities of the transport system play a significant role, and make such tracking studies mandatory.

The *efficiency* of the collimation system must include effects of the interaction of the spoilers and other apertures with the particles themselves. The 'hard-edged' approach of the dynamic aperture studies are unrealistic, since particles are not stopped by a single radiation length of material, but are instead scattered in both angle and energy. By design, most of the scattered particles are outside the aperture of the machine and are stopped in the downstream absorbers: however, a proportion of these scattered particles will be transported through the system and be outside the collimation depth. The collimation efficiency is defined as the fraction of the incident halo population which makes it through the collimation system and is outside the collimation depth at the doublet. The number should be of the order of 10^{-4}, which was achieved for the old system [4]. As of writing, simulations of scattering in the spoilers have not yet been done for the system described here. However section 8 briefly discusses the effects.

The halo was simply modeled as a flat rectangular distribution in five-dimensional phase space, with a transverse extent of $\pm 16.25\sigma_x$ and $\pm 100\sigma_y$ (collimation depth plus 25%). Only about 5% of the particles (~ 5000) actually 'survive' to the entrance of the final doublet: approximately 48% are lost at the momentum (energy) spoiler, with an additional $\sim 40\%$ being lost over the four CDS spoilers. Figure 21 shows the scatter plots of the lost particles at the main (primary) spoilers.

The machine protection philosophy is solely based on protecting the momentum collimator in the event of it being directly hit by a bunch with a large ($> 1.5\%$) momentum error. However, figure 23(a) indicates that $\sim 50\%$ of the tracked halo particles hit the various downstream spoilers; in particular, about 2% survive and strike the secondary collimators in the CCS regions. For the beam halo, this is not particularly significant or dangerous: however, each 'particle' can be considered the centroid of a bunch, which would then hit that collimator. Figure 22 shows the coordinates of the $\sim 10^3$ particles which hit the first spoiler in the vertical CCS, mapped back to the original coordinates at the exit of the linac. If the beam were to exit the linac with one of these coordinates, then that beam would hit the VCCS collimator with
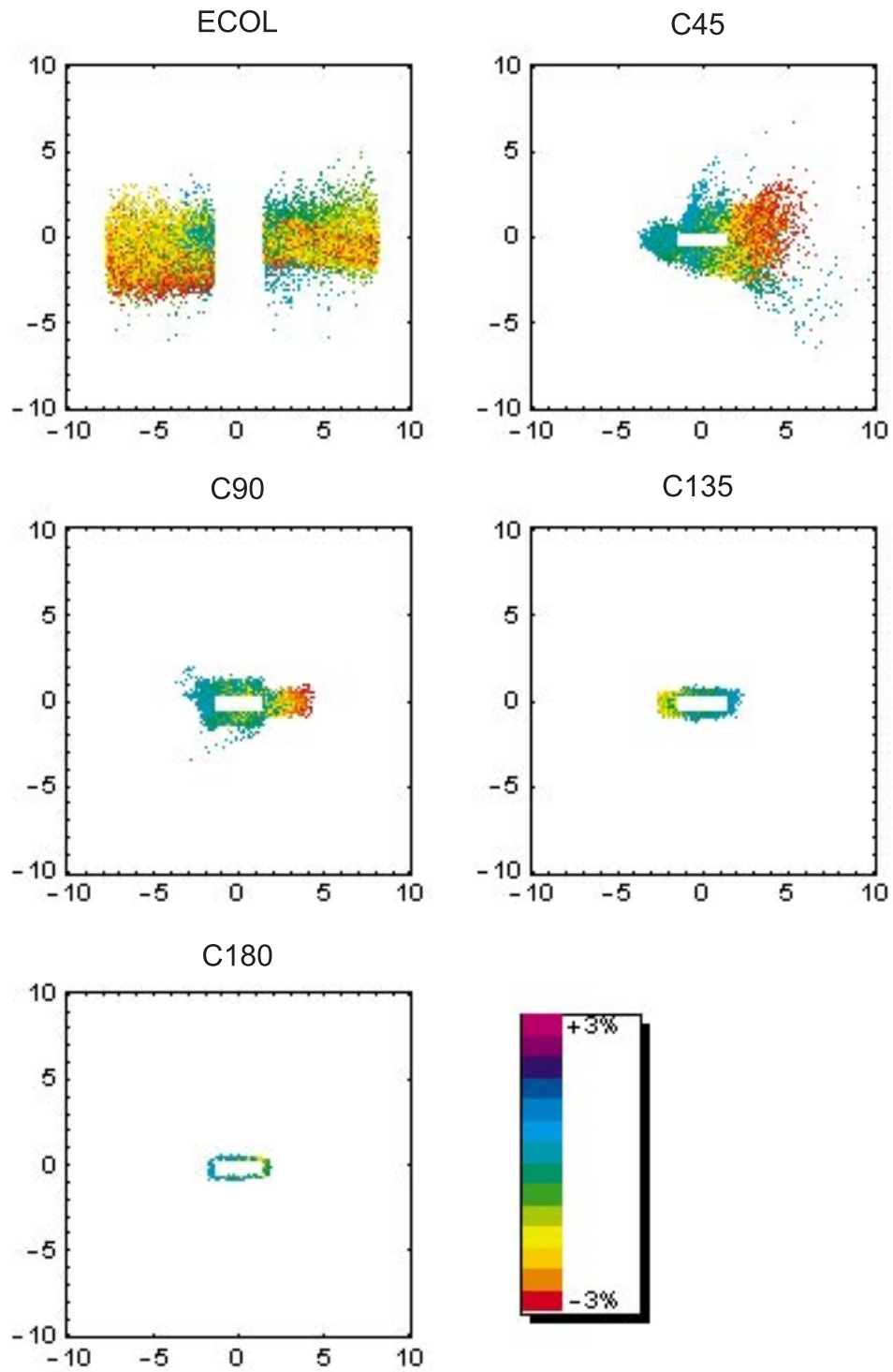
Figure 21: *X-Y scatter plots of the particles lost at the four primary spoilers (collimators). Units are millimeters. The spoiler apertures can be clearly seen. The colour represents the momentum error of the particle ($\Delta p/p$).*
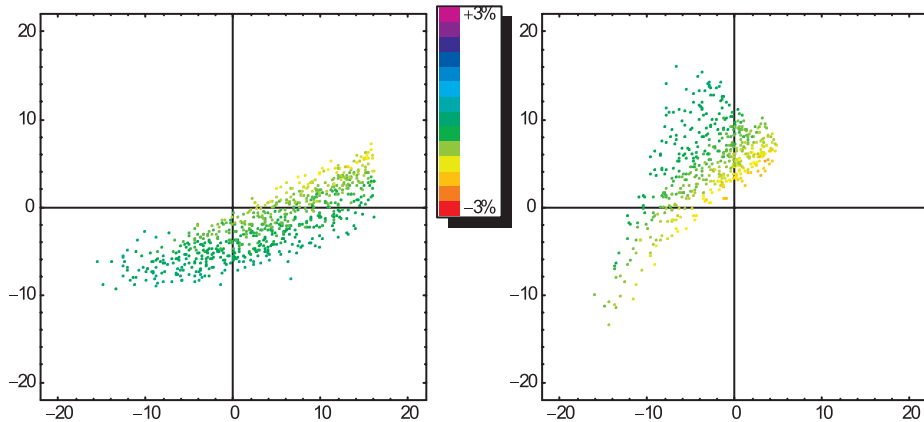
Figure 22: *Horizontal phase space normalised coordinates (x,x') of the ∼ 1% of particles which hit the first spoiler in the vertical CCS, mapped back to the exit of the linac. The left and right plots show respectively those particles which hit the left and right collimator jaw in the VCCS. Units are in linear beam sizes (σ).*

potentially damaging results. Further studies are necessary to evaluate the risk and potential damage of such events.

The ∼2% of the halo which is lost on the CCS collimators is of some concern, since these collimators are intended as *secondary* collimators, and should sit in the shadow of the primary collimation system. Similar tracking studies of the old collimation system [12] indicated that only a few particles in 10^4 were intercepted by these collimators. Furthermore, the original system had only horizontal or vertical spoilers in the corresponding horizontal and vertical CCS sections. For the current system, it was found necessary to have both apertures collimated at both locations, in order to assure no particles outside of the collimation depth at the doublet entrance. The dominant loss is in the horizontal plane — in fact, there are no particles lost on the vertical spoilers in the VCCS section. The exact reasons for this behavior are still under investigation.

Of the initial 10^5 particles, about 2×10^4 (or 20%) are initially inside the (linear) collimation depth[5]. It may therefore seem surprising that only such a small number survive. The strong non-linear terms drive the particle amplitudes outside of the spoiler apertures.

Figure 23 summarises the results of tracking the 10^5 'halo' particles through the BDS. Of the final distribution at the entrance of the doublet (figure 23b), no particles are found outside the required collimation depth.

8   Scattering Effects and Collimation Efficiency

While simulations including scattering in the spoilers and the exact location of the absorbers must still be done, we can make some general statements about what we

---

[5]it is interesting to note that the 'density' of the initial distribution only corresponds to $\sim 10^{-4}$ particle per nominal bunch phase space volume.
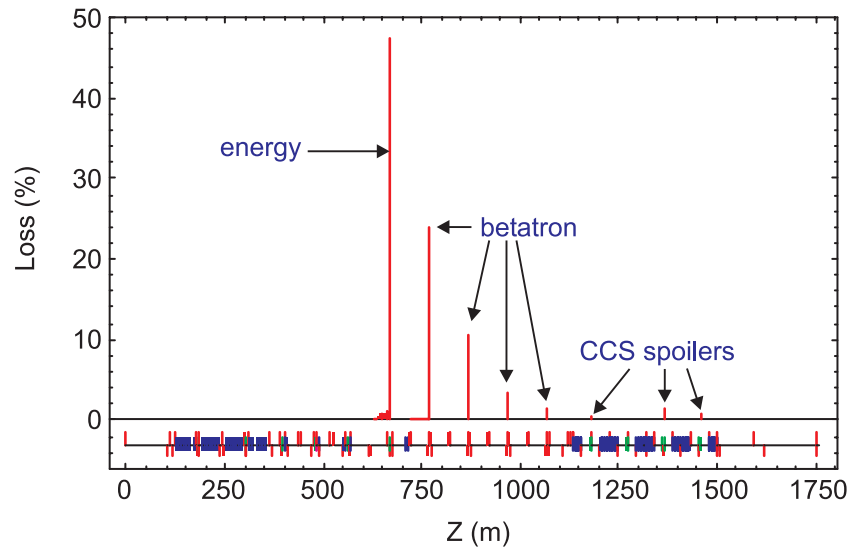
(a) Particles 'losses' along the beamline, expressed as a percentage of the initial particle number tracked.
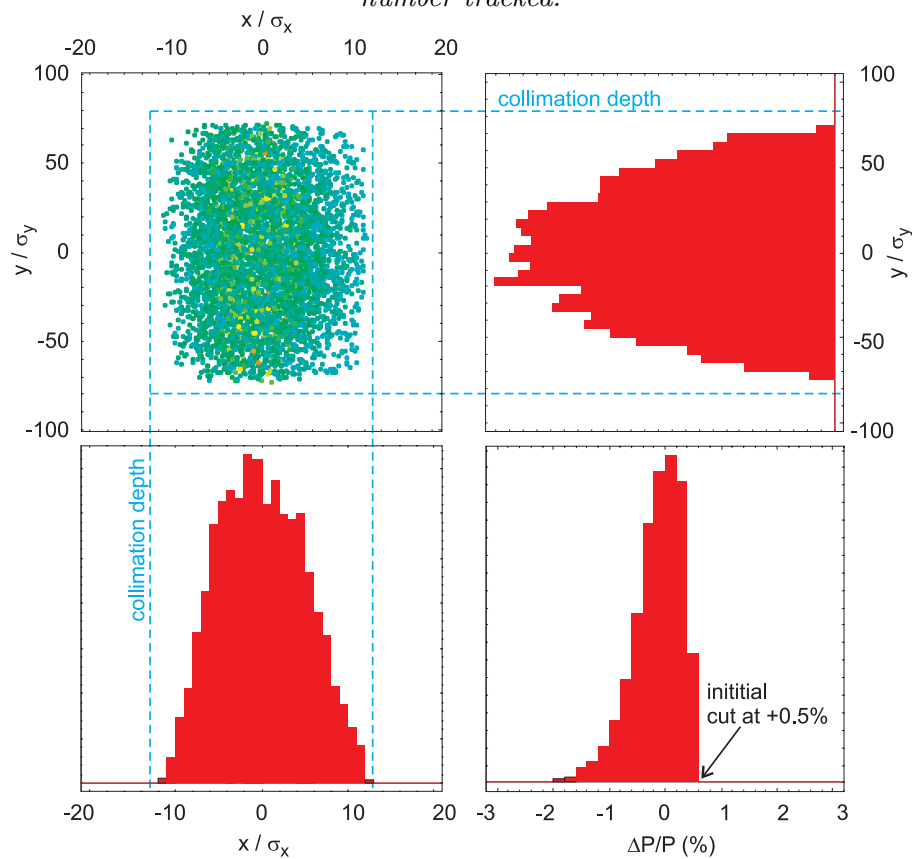
(b) Particle distribution at the entrance to the final doublet after tracking through the entire BDS.

Figure 23: *Results of particle tracking through the BDS. All apertures are treated as 'hard' edges, i.e. a particle outside of a given aperture is deemed lost. An initial flat distribution of 10^5 particles was generated, with a transverse extent of $\pm 16.25\sigma_x$ and $\pm 100\sigma_y$ (collimation depth plus 25%). The momentum distribution was $-3\% < \Delta P/P < +0.5\%$. Effects of scattering and transmission through material are not included.*

expect, based on fundamental knowledge of the scattering mechanisms and the simulations that were done for the original system [4].

As particles travel through the spoiler, they undergo multiple Coulomb scattering which increases their angular spread. The rms angle in a given plane for a spoiler of length L radiation lengths is given by

$$\theta_{rms} \approx \frac{1}{\sqrt{2}} \frac{14.1 \times 10^{-3}}{p[\text{GeV/c}]} \sqrt{L} \tag{10}$$

where p is the momentum of the particle. For $p = 250\,\text{GeV}$ and a one radiation length spoiler, we have $\theta_{rms} \approx 40\,\mu\text{rad}$; this corresponds to $\sim 250\sigma_{x'}$ and $\sim 4570\sigma_{y'}$. If N particles are incident on the spoiler, then we can write the peak scattered particle density as

$$\frac{N}{2\pi \times 250 \times 4570} \approx 1.4 \times 10^{-7} N \tag{11}$$

If we now assume that the aperture defined by the absorber is a factor of two larger than the collimation depth (i.e. $26\sigma_x \times 160\sigma_y$), then we can estimate the number of scattered particles that pass through this aperture as $1.4 \times 10^{-7} \times 26 \times 160 \approx 6 \times 10^{-4} N$.

For a one radiation length spoiler, the average particle energy on exit is $1/e$ of the initial energy, i.e. $\sim 92\,\text{GeV}$ for a $250\,\text{GeV}$ beam. The exact spectrum (in δ) can be estimated from [13]

$$\frac{1}{N} \frac{dN}{d\delta} = \frac{\ln\left(\frac{1}{1-\delta}\right)^{\frac{L}{\ln 2}}}{\Gamma\left(\frac{L}{\ln 2}\right)} \tag{12}$$

where L is again the length in radiation lengths. Figure 24 shows the spectrum for a one radiation length spoiler. The plot shows that about 1% of the scattered particles lose less than 5% of their initial energy. It is highly unlikely that the remaining scattered particles will be transported through the lattice.

Given these scattering effects, we can probably safely assume a collimation efficiency better than 10^{-3}. The exact efficiency must be determined with simulations.

9   Wakefield Effects

For one radiation length of titanium at the specified apertures, the resistive wall wakefield can be ignored. To reduce the geometric wakefield to an acceptable level, the spoilers will be constructed with tapers approximately $1\,\text{m}$ long. Simple estimates based on calculations presented in [4] suggest that vertical beam offsets on the order of a few σ_y cause less than a 2% emittance growth. In addition, recent experimental results from SLAC [14] have shown that such theoretical estimates are pessimistic by as much as a factor of ten. Even with the conservative theoretical estimates, however, there appears to be no significant wakefield effects.
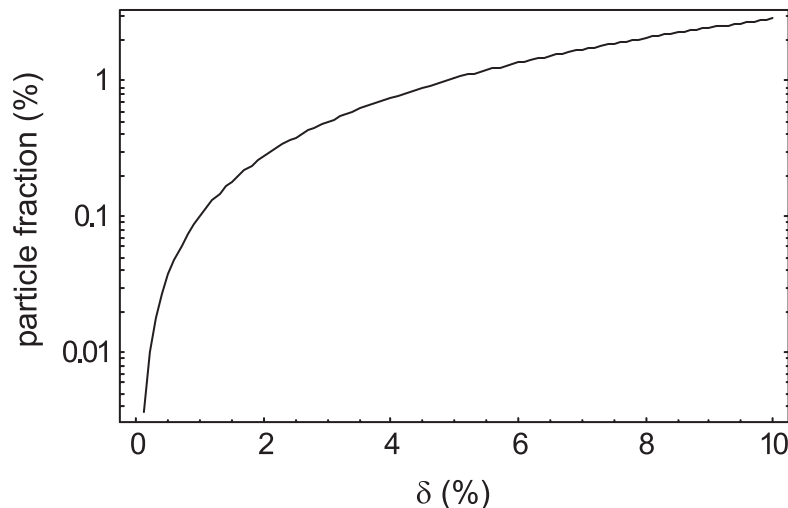
Figure 24: *The integrated $\delta = -\Delta p/p$ spectrum for a one radiation length spoiler. The plot shows the fraction of the scattered particles that are in the range $0 - \delta$.*

10   Summary and Further Work

The post-linac collimation for the proposed TESLA linear collider is designed to remove the halo of the beam to a depth of $13\sigma_x \times 80\sigma_y$, which is defined by the photon acceptance of the IR. The system uses a combination of one radiation length titanium spoilers and 'thick' absorbers placed downstream. A single collimator at a high linear dispersion point $(-100\,\mathrm{mm})$ acts as the primary momentum spoiler, and is followed by four $45°$ cells, with $\beta_x = \beta_y = 800\,\mathrm{m}$ at the symmetry points, where the spoilers are placed. Estimates of the halo from the linac suggest on the order of 10^4 particles per bunch which the system must effectively remove.

Hard-edged (dynamic aperture) tracking studies have shown that no particles exist outside of the defined collimation aperture at the entrance to the IR (entrance of the final doublet). The main momentum collimator is protected from damage from a direct hit by an off-momentum beam by an upstream non-linear system (magnetic energy spoiler, or MES), which couples the horizontal emittance of an off-momentum beam into the vertical plane, and increases the beam size on the spoiler by at least a factor of 6. Studies with GEANT suggest that the spoiler can survive one design bunch, or ~ 6 bunches with the beam size blown up by the MES. The fast emergency extraction line should only allow one or two bunches to pass through before safely extracting the the remainder of the bunch train to the main dump.

The collimation efficiency for the complete system is still to be determined using simulations including scattering of particles from the apertures (spoilers). Additional problems have been identified with respect to primary electrons striking the (nominally) secondary collimators in the chromatic correction sections. The overall safety of the system still needs further risk and analysis work. These problems are currently under investigation.

A   Thin Lens Analysis of the MES System

An off-momentum trajectory with an error $\delta = \Delta p/p$ receives a horizontal kick ($\Delta X'_{\text{oct}}$) from the octupole at the first high dispersion point:

$$\Delta X'_{\text{oct}} \approx \frac{1}{3!} K_3 D_x^3 \delta^3 \tag{13}$$

where K_3 is the integrated (thin-lens) octupole strength, and D_x is the horizontal (linear) dispersion at the octupole. 90° downstream at the second skew-sextupole, this kick generates third-order dispersion:

$$\Delta X_{\text{sext}} \approx \frac{1}{3!} R_{12} K_3 D_x^3 \delta^3 \tag{14}$$

where ΔX_{sext} is the offset at the skew-sextupole, and R_{12} is the linear Green function from the octupole to the skew-sextupole ($= \sqrt{\beta_{x,\text{oct}} \beta_{x,\text{sext}}}$). The momentum-dependent offset of the beam in the skew-sextupole generates a skew-quadrupole with strength K_1:

$$\begin{aligned} K_1 &\approx K_2 \Delta X_{\text{sext}} \\ &\approx \frac{1}{3!} K_2 K_3 R_{12} D_x^3 \delta^3 \end{aligned} \tag{15}$$

The effective skew-quadrupole couples the (large) horizontal emittance into the vertical plane. If we assume that the coupling is strong enough that the vertical divergence of the beam at the sextupole ($\sigma_{y',\text{sext}}$) is dominated by the coupling, we can write the relative increase in vertical beam size at the downstream spoiler as[6]:

$$\begin{aligned} \frac{\sigma_y(\delta)}{\sigma_y(\delta = 0)}\bigg|_{\text{spoiler}} &\approx \frac{\sigma'_y(\delta)}{\sigma'_y(\delta = 0)}\bigg|_{\text{sext}} \\ &\approx K_1 \frac{\sigma_{x,\text{sext}}}{\theta_{y,\text{sext}}} \\ &\approx \frac{1}{3!} K_2 K_3 R_{12} \sqrt{\beta_x \beta_y} \sqrt{\frac{\epsilon_x}{\epsilon_y}} D_x^3 \delta^3 \end{aligned} \tag{16}$$

Equation (16) is the same as equation (4) in section 5.2.

In addition to the induced linear coupling, the skew-sextupole also generates a vertical centroid kick $\Delta Y'_{\text{sext}}$:

$$\begin{aligned} \Delta Y'_{\text{sext}} &= \frac{1}{2} K_2 \Delta X_{\text{sext}}^2 \tag{17} \\ &= \frac{1}{72} K_2 K_3^2 R_{12}^2 D_x^6 \delta^6 \tag{18} \end{aligned}$$

---

[6]implicit in this assumption is that the spoiler is $\pi/2$ downstream of the skew-sextupole in betatron phase in both planes, and that $\alpha_x = \alpha_y = 0$ at both locations

Thus the system generates sixth-order vertical dispersion which then propagates freely through the downstream system. At some momentum error, δ_{crit}, the kick is large enough to cause the beam to just strike a downstream vertical spoiler; this defines a maximum permissible kick, which correspondingly defines a maximum energy-dependent offset at the skew-sextupole (ΔX_{max})[7]. The maximum obtainable beam size increase is then constrained by

$$\left.\frac{\sigma_y(\delta)}{\sigma_y(0)}\right|_{max} \leq \frac{1}{2}K_2\Delta X_{max}\frac{\sigma_x}{\sigma_{y'}} \tag{19}$$

where $\sigma_{y'}$ is now the nominal *design* vertical beam divergence at the skew-sextupole. From equation (17) we can write down the constraint on ΔX_{max}:

$$N_y \geq \frac{1}{2}\frac{K_2\Delta X_{max}^2}{\sigma_{y'}} \tag{20}$$

where N_y is the collimation depth (spoiler aperture) in units of σ_y.

From equations (19) and (20), we have

$$\left.\frac{\sigma_y(\delta)}{\sigma_y(0)}\right|_{max} \leq 2N_y\frac{\sigma_x}{\Delta X_{max}} \tag{21}$$

If we ignore for the moment the momentum spoiler, and consider only those horizontal spoilers in the downstream CDS section where the linear dispersion is zero, then $\Delta X_{max}/\sigma_x \leq N_x$, where N_x is the horizontal collimation depth. Hence we can simplify equation (21) still further:

$$\left.\frac{\sigma_y(\delta)}{\sigma_y(0)}\right|_{max} \leq 2\frac{N_y}{N_x} \tag{22}$$

Thus we arrive at the surprising result that the maximum achievable beam size increase before hitting a spoiler is simply given by the the ratio of the vertical to horizontal normalised collimation apertures. For the current TESLA IR, this amounts to $2 \times 80/13 \approx 12$. The exact value of $\delta = \delta_{crit}$ that this corresponds to depends on the exact choice of parameters. However, we should note that momentum (energy) spoiler (ESPOI) should intercept the beam first, and so the gap is set smaller than $\pm\delta_{crit}/D_{x,\text{spoi}}$, where $D_{x,\text{spoi}}$ is the linear dispersion at the momentum spoiler.

References

[1] N. Merminga, J. Irwin, R. Helm, R. D. Ruth, *Collimation Systems for a TeV Linear Collider*, SLAC-PUB-5165, 1994

[2] R. Brinkmann, G. Materlik, J. Roßbach and A. Wagner (eds.), *Conceptual Design of a 500 GeV e+e- Linear Collider with Integrated X-ray Laser Facility*, DESY-97-048 and ECFA-97-182, chapter 3: http://www.desy.de/lc- cdr/tesla/tesla.html, 1997.

---

[7]From here on we will drop the 'sext' subscript for clarity.

[3] R. Brinkmann et al. (eds.), *The TESLA Technical Design Report*, part II, DESY 2001-011, ECFA 2001-209, DESY TESLA-01-23, DESY TESLA-FEL-01-05, 2001

[4] R. Brinkmann et al., *The TESLA Beam Collimation System*, DESY TESLA-95-25, 1995.

[5] O. Napoly, J. Payet, N. Walker, *Emergency Extraction High-Energy Beamline for TESLA*, DESY TESLA-01-13, 2001.

[6] O. Napoly, *Collimation Depth Requirements for the TESLA IR*, DESY TESLA-01-18, 2001.

[7] C. Stolzenburg, *Untersuchung zur Entstehung von Dunkelstrom in supraleitenden Beschleunigungsstrukturen*, PhD thesis, Hamburg University, 1996

[8] Handbook of Chemistry and Physics, Chemical Rubber Publishing Company, 1976

[9] M.C. Ross et al., *Single Pulse Damage in Copper*, Proc. 20th Int. Linac Conf., Monteray, CA, August 2000 (LINAC2000-MOA06); SLAC-PUB-8605, 2000.

[10] S. Wolfram, *The Mathematica Book*, 3rd ed. Wolfram Media/Cambridge University Press, 1996

[11] N. Walker, *Merlin-II: a C++ Class Library for Charged Particle Accelerator Simulations*, http://www.desy.de/ njwalker/MerlinII, 1999

[12] P. Emma and O. Napoly, *Dynamic Aperture and Collimation in the TESLA Beam Delivery System* DESY TESLA-98-33, 1998

[13] B. Rossi, *High-Energy Particles*, (Prentice-Hall), 1952

[14] P. Tenenbaum et al., *Direct Measurement of Geometric Wakefields from Tapered Rectangular Collimators*, Proc. 20th Int. Linac Conf., Monteray, CA, August 2000 (LINAC2000-MOA09); SLAC-PUB-8563, 2000.